

## 5.1 PART-I: SERIES I

### 5.1.1 Chemistry

#### *5.1.1.1 Synthesis of Series I: Ferulic acid analogues with substituted 3-(4-Hydroxy-3-methoxyphenyl)acrylohydrazide and Series II: Substituted 2-phenyl-1,3,4-oxadiazole tethered with Ferulic acid.*

The target compounds of series I, **5a–o** and series II, **6a–o** were synthesized as per the reaction sequence of Scheme 1 (Chapter 4- Experimental section). Initially, ferulic acid (**1**) was reacted with *N*-hydroxybenzotriazole (HOBT) and 1-ethyl-3-(3-dimethylaminopropyl)carbodiimide hydrochloride (EDC) in acetonitrile to form its ester, which *in situ* reacted with hydrazine hydrate (**2**, 80 %v/v) under cold condition (0–5 °C) to yield 3-(4-hydroxy-3-methoxyphenyl)acrylohydrazide (**3**). The FT-IR spectrum of compound **3** showed the stretching bands at 3654 and 3472 cm<sup>-1</sup> for —OH and —NH functional groups, respectively. Additionally, two stretching vibrations were observed at 3122 and 3117 cm<sup>-1</sup> for NH<sub>2</sub>, which confirmed the formation of hydrazide. The <sup>1</sup>H NMR spectrum showed D<sub>2</sub>O exchangeable peaks at δ<sub>H</sub> 10.60 (1H) and δ<sub>H</sub> 5.41 ppm (2H) for —NH and —NH<sub>2</sub>, respectively. Subsequently, compound **3** was heated under reflux with substituted benzaldehydes (**4a–o**) in ethanol under acidic medium (glacial acetic acid, GAA) to yield respective imines (**5a–o**), which were further cyclized by chloramine T in absolute ethanol to afford molecular hybrids of ferulic acid-based 1,3,4-oxadiazole (**6a–o**). The FT-IR spectra of imines showed characteristic HC=N stretching between 1622–1578 cm<sup>-1</sup>. Also, the disappearance of a dual stretching band of —NH<sub>2</sub> confirmed the formation of imines (**5a–o**). The absence of C=O stretching bands in the FT-IR spectra of compounds **6a–o**, confirmed the cyclization and formation of oxadiazole ring. The disappearance of the D<sub>2</sub>O exchangeable peak of —NH<sub>2</sub> and appearance of HC=N (1H) peak between δ<sub>H</sub> 8.28–8.04 ppm in <sup>1</sup>H NMR

spectra confirmed the formation of imines (**5a–o**). The doublet signals were observed in the range of  $\delta_{\text{H}}$  7.12–7.40 ppm and  $\delta_{\text{H}}$  7.09–6.34 ppm for acrylic **CH=CH** protons of **5a–o**, respectively. The characteristic **HC=N** (1H) and **—NH** (1H) signals were absent in  $^1\text{H}$  NMR spectra of cyclized oxadiazoles (**6a–o**). The similar characteristic doublet signals as observed in **5a–o** were also observed in **6a–o** for acrylic **CH=CH** protons in the range of  $\delta_{\text{H}}$  7.25–7.10 ppm and  $\delta_{\text{H}}$  7.12–6.68 ppm, respectively. In the  $^{13}\text{C}$  NMR spectra, **CH=CH** carbons of **5a–o** were observed at  $\delta_{\text{C}}$  146.11–144.41 ppm and  $\delta_{\text{C}}$  113.10–111.12 ppm, respectively. The similar signals **CH=CH** carbons of **6a–o** were observed at  $\delta_{\text{C}}$  138.34–136.54 ppm and  $\delta_{\text{C}}$  112.14–110.37 ppm, respectively. The  $^{13}\text{C}$  NMR spectra of (**6a–o**) showed two distinguished signals between  $\delta_{\text{C}}$  168.60–165.21 ppm and  $\delta_{\text{C}}$  164.14–154.33 ppm for two carbons present in the oxadiazole ring. The molecular weights of all the target compounds (**5a–o** and **6a–o**) were confirmed by mass spectrometry, and observed fragments were observed as expected with the structural requirements. The percentage purity of synthesized compounds was confirmed to be  $\geq 95\%$  by HPLC.

### 5.1.1.2 Characterization of the synthesized compounds (Series I)

#### 5.1.1.2.1 3-(4-Hydroxy-3-methoxyphenyl)acrylohydrazide (3)

White solid, yield 73%; mp 158–160 °C; TLC (DCM/Methanol 90:10 v/v);  $R_{\text{f}} = 0.32$ . FT-IR ( $\nu \text{ cm}^{-1}$ ): 3654 (**—OH**), 3472 (**—NH**), 3122, 3117 (**—NH<sub>2</sub>**), 1705 (**C=O**).  $^1\text{H}$  NMR (500 MHz)  $\delta_{\text{H}}$  10.60 (s, 1H, **—NH**  $\text{D}_2\text{O}$  exchangeable), 7.37 (d,  $J = 4.2$  Hz, 1H), 7.28–7.22 (m, 2H), 7.16 (d,  $J = 7.5$  Hz, 1H), 7.14 (d,  $J = 1.2$  Hz, 1H), 5.41 (s, 2H, **—NH<sub>2</sub>**  $\text{D}_2\text{O}$  exchangeable), 4.16 (s, 1H), 4.01 (s, 3H).

#### 5.1.1.2.2 *N'*-(Benzylidene)-3-(4-hydroxy-3-methoxyphenyl) acrylohydrazide (5a)

White solid, yield 85%; mp 190–192 °C; TLC (DCM/Methanol 90:10 v/v);  $R_{\text{f}} = 0.62$ . FT-IR ( $\nu \text{ cm}^{-1}$ ): 3650 (**—OH**), 3246 (**—NH**), 1688 (**C=O**), 1610 (**C=N**).  $^1\text{H}$  NMR (500

MHz)  $\delta_{\text{H}}$  10.33 (s, 1H, —NH, D<sub>2</sub>O exchangeable), 8.13 (s, 1H), 7.57 (d,  $J = 10.2$  Hz, 1H), 7.45–7.38 (m, 3H), 7.24–7.18 (m, 2H), 7.08–7.01 (m, 2H), 6.86 (d,  $J = 7.5$  Hz, 1H), 6.56 (d,  $J = 8.2$  Hz, 1H), 3.91 (s, 1H), 3.83 (s, 3H). <sup>13</sup>C NMR (126 MHz)  $\delta_{\text{C}}$  161.56, 149.14, 148.50, 145.81, 144.64, 129.07, 128.74, 127.58, 127.03, 123.18, 122.28, 115.81, 111.77, 56.78. LC/MS (ESI,  $m/z$ ): 297 [M + H]<sup>+</sup>. HPLC purity: 98.17%, retention time: 3.10 min.

**5.1.1.2.3. *N'*-(2,3-Dimethoxybenzylidene)-3-(4-hydroxy-3-methoxyphenyl)acrylohydrazide (5b)**

White solid, yield 89% (Reaction time: 7 h); mp 182–184 °C; TLC (DCM/Methanol 90:10 v/v);  $R_{\text{f}} = 0.59$ . FT-IR ( $\nu$  cm<sup>-1</sup>): 3668 (—OH), 3255 (—NH), 1710 (C=O), 1602 (C=N). <sup>1</sup>H NMR (500 MHz)  $\delta_{\text{H}}$  10.41 (s, 1H, —NH, D<sub>2</sub>O exchangeable), 8.16 (s, 1H), 7.40 (d,  $J = 11.8$  Hz, 1H), 7.00 (s, 1H), 6.95 (s, 1H), 6.91 (t,  $J = 5.8$  Hz, 3H), 6.73 (s, 1H), 6.34 (d,  $J = 8.8$  Hz, 1H), 3.96 (s, 1H), 3.84 (s, 9H). <sup>13</sup>C NMR (126 MHz)  $\delta_{\text{C}}$  163.10, 154.00, 149.57, 148.50, 147.70, 145.81, 140.65, 131.42, 127.58, 123.20, 122.28, 115.81, 111.77, 106.73, 60.65, 57.05. LC/MS (ESI,  $m/z$ ): 387 [M + H]<sup>+</sup>. HPLC purity: 98.80%, retention time: 2.54 min.

**5.1.1.2.4. 3-(4-Hydroxy-3-methoxyphenyl)-*N'*-(3,4,5-trimethoxybenzylidene)acrylohydrazide (5c)**

White solid, yield 74%; mp 168–170 °C; TLC (DCM/Methanol 90:10 v/v);  $R_{\text{f}} = 0.57$ . FT-IR ( $\nu$  cm<sup>-1</sup>): 3673 (—OH), 3262 (—NH), 1705 (C=O), 1605 (C=N). <sup>1</sup>H NMR (500 MHz)  $\delta_{\text{H}}$  10.48 (s, 1H, —NH, D<sub>2</sub>O exchangeable), 8.15 (s, 1H), 7.49 (d,  $J = 11.4$  Hz, 1H), 7.12 (d,  $J = 1.5$  Hz, 1H), 6.98 (dd,  $J = 5.4, 1.4$  Hz, 1H), 6.92 (d,  $J = 7.5$  Hz, 1H), 6.71 (s, 2H), 6.38 (d,  $J = 8.2$  Hz, 1H), 3.94 (s, 1H), 3.83 (s, 3H), 3.81 (s, 9H). <sup>13</sup>C NMR (126 MHz)  $\delta_{\text{C}}$  163.10, 154.00, 149.57, 148.50, 147.70, 145.81, 140.65, 131.42, 127.58,

123.20, 122.28, 115.81, 111.77, 106.73, 60.65, 57.05. LC/MS (ESI,  $m/z$ ): 387  $[M + H]^+$ .  
HPLC purity: 98.80%, retention time: 2.52 min.

**5.1.1.2.5.** ***3-(4-Hydroxy-3-methoxyphenyl)-N'-(4-hydroxybenzylidene)acrylohydrazide (5d)***

White solid, yield 78%; mp 174-176 °C; TLC (DCM/Methanol 90:10 v/v);  $R_f = 0.62$ .  
FT-IR ( $\nu$   $\text{cm}^{-1}$ ): 3642 (—OH), 3228 (—NH), 1674 (C=O), 1618 (C=N).  $^1\text{H}$  NMR (500 MHz)  $\delta_{\text{H}}$  10.21 (s, 1H, —NH,  $\text{D}_2\text{O}$  exchangeable), 8.11 (s, 1H), 7.52 (d,  $J = 10.6$  Hz, 1H), 7.08 (d,  $J = 7.1$  Hz, 2H), 7.04 (dd,  $J = 6.4, 1.6$  Hz, 1H), 7.00 (dd,  $J = 4.5, 3.0$  Hz), 6.82 (d,  $J = 7.4$  Hz, 1H), 6.42 (d,  $J = 8.8$  Hz, 1H), 3.96 (s, 1H), 3.88 (s, 1H), 3.72 (s, 3H).  $^{13}\text{C}$  NMR (126 MHz)  $\delta_{\text{C}}$  162.54, 158.12, 149.21, 149.14, 148.62, 145.11, 128.82, 127.53, 126.92, 123.18, 121.58, 116.82, 115.01, 111.12, 54.70. LC/MS (ESI,  $m/z$ ): 313  $[M + H]^+$ . HPLC purity: 95.30%, retention time: 3.41 min.

**5.1.1.2.6.** ***3-(4-Hydroxy-3-methoxyphenyl)-N'-(2-hydroxybenzylidene)acrylohydrazide (5e)***

White solid, yield 80%; mp 175-177 °C; TLC (DCM/Methanol 90:10 v/v);  $R_f = 0.59$ .  
FT-IR ( $\nu$   $\text{cm}^{-1}$ ): 3650 (—OH), 3246 (—NH), 1688 (C=O), 1615 (C=N).  $^1\text{H}$  NMR (500 MHz)  $\delta_{\text{H}}$  10.26 (s, 1H, —NH,  $\text{D}_2\text{O}$  exchangeable), 8.14 (s, 1H), 7.44 (d,  $J = 10.8$  Hz, 1H), 7.28 (t,  $J = 7.2, 1.2$  Hz, 1H), 7.07–6.99 (m, 4H), 6.89–6.84 (m, 2H), 6.56 (d,  $J = 8.4$  Hz, 1H), 4.21 (s, 1H), 3.93 (d,  $J = 5.5$  Hz, 4H).  $^{13}\text{C}$  NMR (126 MHz)  $\delta_{\text{C}}$  162.52, 158.32, 150.38, 149.57, 148.50, 145.81, 129.75, 128.54, 127.58, 123.85, 122.28, 121.19, 120.39, 117.37, 115.81, 111.77, 55.15. LC/MS (ESI,  $m/z$ ): 313  $[M + H]^+$ . HPLC purity: 96.45%, retention time: 3.56 min.

**5.1.1.2.7. *N'*-(-2,4-Dihydroxybenzylidene)-3-(4-hydroxy-3-methoxyphenyl)acrylohydrazide (5f)**

White solid, yield 83%; mp 179-181 °C; TLC (DCM/Methanol 90:10 v/v);  $R_f = 0.54$ . FT-IR ( $\nu$   $\text{cm}^{-1}$ ): 3668 (—OH), 3264 (—NH), 1680 (C=O), 1622 (C=N).  $^1\text{H}$  NMR (500 MHz)  $\delta_{\text{H}}$  10.34 (s, 1H, —NH  $\text{D}_2\text{O}$  exchangeable), 8.17 (s, 1H), 7.54 (d,  $J = 11.8$  Hz, 1H), 7.08–7.03 (m, 2H), 6.80 (d,  $J = 7.4$  Hz, 1H), 6.72 (d,  $J = 7.5$  Hz, 1H), 6.65 (d,  $J = 7.0$ , 1H), 6.50 (dd,  $J = 8.2, 6.8$  Hz, 2H), 4.21 (s, 1H), 3.97 (s, 1H), 3.82 (d,  $J = 5.7$  Hz, 4H).  $^{13}\text{C}$  NMR (126 MHz)  $\delta_{\text{C}}$  163.62, 160.51, 150.38, 149.57, 148.50, 145.81, 130.86, 127.58, 123.18, 122.28, 115.81, 113.18, 111.77, 109.20, 103.04, 56.78. LC/MS (ESI,  $m/z$ ): 329  $[\text{M} + \text{H}]^+$ . HPLC purity: 96.49%, retention time: 4.50 min.

**5.1.1.2.8. 3-(4-Hydroxy-3-methoxyphenyl)-*N'*-(-3-methylbenzylidene)acrylohydrazide (5g)**

White solid, yield 73%; mp 188-190 °C; TLC (DCM/Methanol 90:10 v/v);  $R_f = 0.58$ . FT-IR ( $\nu$   $\text{cm}^{-1}$ ): 3688 (—OH), 3284 (—NH), 1688 (C=O), 1582 (C=N).  $^1\text{H}$  NMR (500 MHz)  $\delta_{\text{H}}$  10.12 (s, 1H, —NH,  $\text{D}_2\text{O}$  exchangeable), 8.09 (s, 1H), 7.59 (d,  $J = 10.5$  Hz, 1H), 7.39–7.36 (m, 2H), 7.16 (t,  $J = 8.2, 1.4$  Hz, 1H), 6.98–6.91 (m, 2H), 6.86 (d,  $J = 6.2$  Hz, 1H), 6.80 (t,  $J = 6.0, 1.8$  Hz, 1H), 6.56 (d,  $J = 10.4$  Hz, 1H), 3.88 (s, 1H), 3.72 (s, 3H), 2.40 (s, 3H).  $^{13}\text{C}$  NMR (126 MHz)  $\delta_{\text{C}}$  161.49, 149.57, 149.18, 148.52, 145.81, 137.80, 136.54, 129.71, 128.53, 128.19, 127.58, 123.54, 123.10, 122.28, 111.81, 107.25, 56.78, 21.20. LC/MS (ESI,  $m/z$ ): 311  $[\text{M} + \text{H}]^+$ . HPLC purity: 98.80%, retention time: 4.0 min.

**5.1.1.2.9. 3-(4-Hydroxy-3-methoxyphenyl)-*N'*-(-4-methylbenzylidene)acrylohydrazide (5h)**

White solid, yield 77%; mp 168-170 °C; TLC (DCM/Methanol 90:10 v/v);  $R_f = 0.53$ . FT-IR ( $\nu$   $\text{cm}^{-1}$ ): 3634 (—OH), 3218 (—NH), 1672 (C=O), 1604 (C=N).  $^1\text{H}$  NMR (500

MHz)  $\delta_{\text{H}}$  10.09 (s, 1H, —NH D<sub>2</sub>O exchangeable), 8.04 (s, 1H), 7.51 (d,  $J = 11.9$  Hz, 1H), 7.29 (d,  $J = 5.4$  Hz, 2H), 7.17 (d,  $J = 7.5$  Hz, 2H), 7.07–7.04 (m, 2H), 6.64 (d,  $J = 7.0$  Hz, 1H), 6.56 (d,  $J = 7.5$  Hz, 1H), 3.92 (s, 1H), 3.85 (s, 3H), 2.31 (s, 3H). <sup>13</sup>C NMR (126 MHz)  $\delta_{\text{C}}$  161.54, 149.57, 149.14, 148.50, 145.85, 138.51, 131.90, 129.15, 127.58, 127.35, 123.18, 122.28, 115.81, 112.77, 56.78, 21.12. LC/MS (ESI,  $m/z$ ): 311 [M + H]<sup>+</sup>. HPLC purity: 97.40%, retention time: 5.64 min.

**5.1.1.2.10. 3-(4-Hydroxy-3-methoxyphenyl)-N'-(4-nitrobenzylidene)acrylohydrazide (5i)**

White solid, yield 78%; mp 188–190 °C; TLC (DCM/Methanol 90:10 v/v);  $R_{\text{f}} = 0.69$ . FT-IR ( $\nu$  cm<sup>-1</sup>): 3690 (—OH), 3278 (—NH), 1730 (C=O), 1615 (C=N). <sup>1</sup>H NMR (500 MHz)  $\delta_{\text{H}}$  10.61 (s, 1H, —NH D<sub>2</sub>O exchangeable), 8.28 (d,  $J = 7.5$  Hz, 2H), 8.06 (s, 1H), 7.71 (dd,  $J = 15.5, 11.3$  Hz, 2H), 7.58 (d,  $J = 11.4$  Hz, 1H), 7.42–6.39 (m, 2H), 6.81 (d,  $J = 6.1$  Hz, 1H), 6.66 (d,  $J = 3.5$  Hz, 1H), 4.34 (s, 1H), 3.90 (s, 3H). <sup>13</sup>C NMR (126 MHz)  $\delta_{\text{C}}$  163.01, 151.52, 151.14, 148.59, 148.02, 145.32, 139.14, 127.01, 124.48, 123.18, 122.28, 115.81, 112.54, 59.41. LC/MS (ESI,  $m/z$ ): 342 [M + H]<sup>+</sup>. HPLC purity: 97.13%, retention time: 3.21 min.

**5.1.1.2.11. 3-(4-Hydroxy-3-methoxyphenyl)-N'-(4-(trifluoromethyl)benzylidene)acrylohydrazide (5j)**

White solid, yield 73%; mp 176–178 °C; TLC (DCM/Methanol 90:10 v/v);  $R_{\text{f}} = 0.61$ . FT-IR ( $\nu$  cm<sup>-1</sup>): 3702 (—OH), 3285 (—NH), 1715 (C=O), 1578 (C=N). <sup>1</sup>H NMR (500 MHz)  $\delta_{\text{H}}$  10.10 (s, 1H, —NH D<sub>2</sub>O exchangeable), 8.26 (s, 1H), 8.08 (d,  $J = 10.8$  Hz, 1H), 7.86 (t,  $J = 6.4, 1.2$  Hz, 2H), 7.63–7.57 (m, 1H), 7.51 (d, 2H), 7.44–6.85 (m, 2H), 6.64 (d,  $J = 8.2$  Hz, 1H), 4.24 (s, 1H), 3.84 (d,  $J = 10.0$  Hz, 3H). <sup>13</sup>C NMR (126 MHz)  $\delta_{\text{C}}$  162.57, 149.44, 149.30, 148.34, 145.02, 130.34 (q,  $J_{\text{C-F}} = 28.2$  Hz), 129.33, 129.20, 122.50 (q,  $J_{\text{C-F}} = 5.1$  Hz), 121.52, 119.48 (q,  $J_{\text{C-F}} = 261.5$  Hz), 113.96, 112.72, 111.52,

56.26, 56.02. LC/MS (ESI,  $m/z$ ): 365  $[M + H]^+$ . HPLC purity: 99.81%, retention time: 3.0 min.

**5.1.1.2.12.** *3-(4-Hydroxy-3-methoxyphenyl)-N'-(4-(trifluoromethoxy)benzylidene)acrylohydrazide (5k)*

White solid, yield 76%; mp 172–174 °C; TLC (DCM/Methanol 90:10 v/v);  $R_f = 0.67$ . FT-IR ( $\nu$   $\text{cm}^{-1}$ ): 3708 (—OH), 3294 (—NH), 1722 (C=O), 1590 (C=N).  $^1\text{H}$  NMR (500 MHz)  $\delta_{\text{H}}$  10.11 (s, 1H, —NH,  $\text{D}_2\text{O}$  exchangeable), 8.30 (s, 1H), 8.12 (d,  $J = 11.2$  Hz, 1H), 7.92 (t,  $J = 7.4, 2.2$ , 2H), 7.78 (d,  $J = 8.2$  Hz, 2H), 7.65–7.43 (m, 1H), 7.43–7.09 (m, 3H), 4.24 (s, 1H), 3.84 (d,  $J = 15.2$  Hz 3H).  $^{13}\text{C}$  NMR (126 MHz)  $\delta_{\text{C}}$  162.69, 149.37, 148.34, 144.84, 143.66, 142.10, 141.55, 138.87, 128.03, 127.91, 126.55, 126.11, 126.08, 125.67, 119.78 (q,  $J_{\text{C-F}} = 242.7$  Hz), 113.82, 112.66, 111.53, 56.24, 56.01. LC/MS (ESI,  $m/z$ ): 381  $[M + H]^+$ . HPLC purity: 99.19%, retention time: 3.10 min.

**5.1.1.2.13.** *N'-(4-Chlorobenzylidene)-3-(4-hydroxy-3-methoxyphenyl)acrylohydrazide (5l)*

White solid, yield 81%; mp 168–170 °C; TLC (DCM/Methanol 90:10 v/v);  $R_f = 0.59$ . FT-IR ( $\nu$   $\text{cm}^{-1}$ ): 3702 (—OH), 3277 (—NH), 1709 (C=O), 1594 (C=N).  $^1\text{H}$  NMR (500 MHz)  $\delta_{\text{H}}$  10.42 (s, 1H, —NH,  $\text{D}_2\text{O}$  exchangeable), 8.16 (s, 1H), 7.67 (d,  $J = 11.2$  Hz, 1H), 7.53 (d,  $J = 4.2$  Hz, 2H), 7.12 (d,  $J = 3.5$  Hz, 2H), 7.10–7.06 (m, 2H), 6.92 (d,  $J = 7.5$  Hz, 1H), 6.49 (d,  $J = 8.2$  Hz, 1H), 4.02 (s, 1H), 3.94 (s, 3H).  $^{13}\text{C}$  NMR (126 MHz)  $\delta_{\text{C}}$  163.05, 150.51, 149.10, 148.25, 144.41, 134.15, 129.60, 126.24, 123.18, 121.26, 114.41, 112.58, 59.10. LC/MS (ESI,  $m/z$ ): 331  $[M + H]^+$ . HPLC purity: 98.90%, retention time: 3.94 min.

**5.1.1.2.14. *N'*-(2,4-Dichlorobenzylidene)-3-(4-hydroxy-3-methoxyphenyl)acrylohydrazide (5m)**

White solid, yield 84%; mp 162–164 °C; TLC (DCM/Methanol 90:10 v/v);  $R_f = 0.68$   
FT-IR ( $\nu$   $\text{cm}^{-1}$ ): 3714 (—OH), 3284 (—NH), 1718 (C=O), 1606 (C=N).  $^1\text{H}$  NMR (500 MHz)  $\delta_{\text{H}}$  10.51 (s, 1H, —NH,  $\text{D}_2\text{O}$  exchangeable), 8.15 (s, 1H), 7.91 (s, 1H), 7.58 (d,  $J = 11.4$  Hz, 1H), 7.41 (d,  $J = 1.6$  Hz, 1H), 7.04 (dd,  $J = 7.4, 3.1$  Hz, 3H), 6.89 (d,  $J = 7.4$  Hz, 1H), 6.74 (d,  $J = 7.3$  Hz, 1H), 4.20 (s, 1H), 4.12 (s, 3H).  $^{13}\text{C}$  NMR (126 MHz)  $\delta_{\text{C}}$  163.41, 150.20, 149.46, 146.68, 145.53, 132.13, 131.21, 128.91, 124.52, 121.28, 116.81, 112.70, 60.52. LC/MS (ESI,  $m/z$ ): 365  $[\text{M} + \text{H}]^+$ . HPLC purity: 97.45%, retention time: 5.74 min.

**5.1.1.2.15. *N'*-(4-Fluorobenzylidene)-3-(4-hydroxy-3-methoxyphenyl) acrylohydrazide (5n)**

White solid, yield 88%; mp 177–180 °C; TLC (DCM/Methanol 90:10 v/v);  $R_f = 0.67$ .  
FT-IR ( $\nu$   $\text{cm}^{-1}$ ): 3710 (—OH), 3279 (—NH), 1714 (C=O), 1618 (C=N).  $^1\text{H}$  NMR (500 MHz)  $\delta_{\text{H}}$  10.46 (s, 1H, —NH,  $\text{D}_2\text{O}$  exchangeable), 8.14 (s, 1H), 7.86 (d,  $J = 15.2$  Hz, 1H), 7.63 (t,  $J = 7.7$  Hz, 2H), 7.44–7.40 (m, 2H), 7.18–7.15 (m, 2H), 6.90 (d,  $J = 7.5$  Hz, 1H), 6.61 (d,  $J = 7.5$  Hz, 1H), 4.10 (s, 1H), 4.07 (s, 3H).  $^{13}\text{C}$  NMR (126 MHz)  $\delta_{\text{C}}$  162.81 (d,  $J_{\text{C-F}} = 228.7$  Hz), 161.10, 160.83, 150.21, 149.04, 148.50, 146.11, 131.12 (d,  $J_{\text{C-F}} = 4.5$  Hz), 130.37 (d,  $J_{\text{C-F}} = 8.2$  Hz), 127.18, 122.28, 115.62 (d,  $J_{\text{C-F}} = 12.5$  Hz), 113.10, 58.98. LC/MS (ESI,  $m/z$ ): 315  $[\text{M} + \text{H}]^+$ . HPLC purity: 98.90%, retention time: 3.95 min.

**5.1.1.2.16. *N'*-(2,4-Difluorobenzylidene)-3-(4-hydroxy-3-methoxyphenyl)acrylohydrazide (5o)**

White solid, yield 83%; mp 181–183 °C; TLC (DCM/Methanol 90:10 v/v);  $R_f = 0.64$ .  
FT-IR ( $\nu$   $\text{cm}^{-1}$ ): 3730 (—OH), 3296 (—NH), 1728 (C=O), 1607 (C=N).  $^1\text{H}$  NMR (500



MHz)  $\delta_{\text{H}}$  10.58 (s, 1H, —NH, D<sub>2</sub>O exchangeable), 8.19 (s, 1H), 7.71 (d,  $J = 8.4$  Hz, 1H), 7.46 (t,  $J = 7.9, 0.9$  Hz, 1H), 7.12–7.08 (m, 2H), 7.00 (d,  $J = 1.5$  Hz, 2H), 6.91–6.88 (m, 1H), 6.37 (d,  $J = 5.7$  Hz, 1H), 4.15 (s, 1H), 4.09 (s, 3H). <sup>13</sup>C NMR (126 MHz)  $\delta_{\text{C}}$  163.82, 163.47 (d,  $J_{\text{C-F}} = 279.7$  Hz), 162.78 (d,  $J_{\text{C-F}} = 7.6$  Hz), 161.38 (d,  $J_{\text{C-F}} = 284.5$  Hz), 160.68 (d,  $J_{\text{C-F}} = 5.2$  Hz), 149.57, 149.04 (d,  $J_{\text{C-F}} = 3.2$  Hz), 148.90, 148.50, 145.81, 132.90 (t,  $J_{\text{C-F}} = 7.1$  Hz), 127.55, 123.18, 122.28, 120.35, 120.13, 115.81, 113.05 (d,  $J = 4.7$  Hz), 112.83 (d,  $J_{\text{C-F}} = 4.5$  Hz), 103.58, 60.28. LC/MS (ESI,  $m/z$ ): 333 [M + H]<sup>+</sup>. HPLC purity: 97.14%, retention time: 5.19 min.

**5.1.1.2.17. 2-Methoxy-4-(2-(5-phenyl-1,3,4-oxadiazol-2-yl)vinyl)phenol (6a)**

White solid, yield 84%; mp 118–120 °C; TLC (DCM/Methanol 90:10 v/v);  $R_{\text{f}} = 0.74$ . FT-IR ( $\nu$  cm<sup>-1</sup>): 3690 (—OH). <sup>1</sup>H NMR (500 MHz)  $\delta_{\text{H}}$  7.56 (d,  $J = 7.4, 1.4$  Hz, 2H), 7.41 (t,  $J = 7.3$  Hz, 2H), 7.36–7.32 (m, 1H), 7.10 (d,  $J = 10.2$  Hz, 1H), 6.86 (d,  $J = 4.5$  Hz, 1H), 6.81–6.77 (m, 2H), 6.68 (d,  $J = 7.2$  Hz, 1H), 3.95 (s, 1H), 3.82 (s, 3H). <sup>13</sup>C NMR (126 MHz)  $\delta_{\text{C}}$  166.60, 163.88, 149.57, 148.50, 137.85, 131.56, 129.05, 127.58, 127.08, 126.66, 123.18, 115.81, 111.77, 110.13, 55.21. LC/MS (ESI,  $m/z$ ): 295 [M + H]<sup>+</sup>. HPLC purity: 98.0%, retention time: 6.35 min.

**5.1.1.2.18. 4-(2-(5-(2,3-Dimethoxyphenyl)-1,3,4-oxadiazol-2-yl)vinyl)-2-methoxyphenol (6b)**

White solid, yield 82%; mp 113–115 °C; TLC (DCM/Methanol 90:10 v/v);  $R_{\text{f}} = 0.81$ . FT-IR ( $\nu$  cm<sup>-1</sup>): 3664 (—OH). <sup>1</sup>H NMR (500 MHz)  $\delta_{\text{H}}$  7.19 (d,  $J = 6.8$ , 1H), 7.14 (d,  $J = 11.4$  Hz, 1H), 7.05 (t,  $J = 7.5$  Hz, 1H), 6.92 (d,  $J = 3.4$  Hz, 1H), 6.83–6.79 (m, 2H), 6.77 (d,  $J = 4.1$  Hz, 1H), 6.70 (d,  $J = 7.5$  Hz, 1H), 4.30 (s, 1H), 4.19 (s, 6H). <sup>13</sup>C NMR (126 MHz)  $\delta_{\text{C}}$  166.13, 163.57, 153.25, 150.42, 148.21, 136.52, 123.99, 120.36, 117.90, 114.61, 110.24, 60.95, 55.18. LC/MS (ESI,  $m/z$ ): 355 [M + H]<sup>+</sup>. HPLC purity: 97.10%, retention time: 5.44 min.

**5.1.1.2.19. 2-Methoxy-4-(2-(5-(3,4,5-trimethoxyphenyl)-1,3,4-oxadiazol-2-yl)vinyl)phenol (6c)**

White solid, yield 86%; mp 109–111 °C; TLC (DCM/Methanol 90:10 v/v);  $R_f = 0.84$ . FT-IR ( $\nu$   $\text{cm}^{-1}$ ): 3658 (—OH).  $^1\text{H}$  NMR (500 MHz)  $\delta_{\text{H}}$  7.09 (d,  $J = 10.3$  Hz, 1H), 6.88–6.84 (m, 2H), 6.81–6.78 (m, 3H), 6.68 (d,  $J = 7.8$  Hz, 1H), 4.29 (s, 1H), 4.15 (s, 9H).  $^{13}\text{C}$  NMR (126 MHz)  $\delta_{\text{C}}$  166.03, 163.43, 151.61, 149.57, 143.55, 137.82, 127.58, 123.18, 122.02, 114.24, 110.39, 110.13, 107.03, 59.36, 54.28. LC/MS (ESI,  $m/z$ ): 385  $[\text{M} + \text{H}]^+$ . HPLC purity: 95.46%, retention time: 2.13 min.

**5.1.1.2.20. 4-(2-(5-(4-Hydroxyphenyl)-1,3,4-oxadiazol-2-yl)vinyl)-2-methoxyphenol (6d)**

White solid, yield 89%; mp 112–114 °C; TLC (DCM/Methanol 90:10 v/v);  $R_f = 0.68$ . FT-IR ( $\nu$   $\text{cm}^{-1}$ ): 3674 (—OH).  $^1\text{H}$  NMR (500 MHz)  $\delta_{\text{H}}$  7.40 (d,  $J = 7.5$  Hz, 2H), 7.01 (d,  $J = 10.2$  Hz, 1H), 6.91 (d,  $J = 7.5$  Hz, 2H), 6.86 (d,  $J = 6.4$  Hz, 1H), 6.83–6.80 (m, 2H), 6.74 (d,  $J = 7.3$  Hz, 1H), 4.91 (s, 1H), 4.45 (s, 1H), 4.21 (s, 3H).  $^{13}\text{C}$  NMR (126 MHz)  $\delta_{\text{C}}$  167.21, 163.89, 160.80, 150.57, 148.50, 138.72, 127.69, 122.52, 117.41, 115.91, 111.78, 110.14, 56.79. LC/MS (ESI,  $m/z$ ): 311  $[\text{M} + \text{H}]^+$ . HPLC purity: 96.82%, retention time: 3.28 min.

**5.1.1.2.21. 4-(2-(5-(2-Hydroxyphenyl)-1,3,4-oxadiazol-2-yl)vinyl)-2-methoxyphenol (6e)**

White solid, yield 78%; mp 122–124 °C; TLC (DCM/Methanol 90:10 v/v);  $R_f = 0.74$ . FT-IR ( $\nu$   $\text{cm}^{-1}$ ): 3681 (—OH).  $^1\text{H}$  NMR (500 MHz)  $\delta_{\text{H}}$  7.48 (s, 1H), 7.39 (dd,  $J = 7.4$ , 1.8 Hz, 1H), 7.18 (d,  $J = 10.5$ , 1H), 7.13 (d,  $J = 6.2$  Hz, 1H), 6.98 (t,  $J = 7.5$ , 1.4 Hz, 2H), 6.92–6.84 (m, 2H), 6.68 (d,  $J = 3.2$ , 1H), 4.74 (s, 1H), 4.28 (s, 1H), 4.18 (s, 3H).  $^{13}\text{C}$  NMR (126 MHz)  $\delta_{\text{C}}$  167.65, 158.44, 154.72, 149.57, 147.25, 137.82, 131.78,

130.11, 127.78 123.18, 119.86, 118.80, 115.81, 110.13, 57.36. LC/MS (ESI,  $m/z$ ): 311 [M + H]<sup>+</sup>. HPLC purity: 96.13%, retention time: 2.94 min.

**5.1.1.2.22. 4-(5-(4-Hydroxy-3-methoxystyryl)-1,3,4-oxadiazol-2-yl)benzene-1,3-diol (6f)**

White solid, yield 71%; mp 104–106 °C; TLC (DCM/Methanol 90:10 v/v);  $R_f$  = 0.69. FT-IR ( $\nu$  cm<sup>-1</sup>): 3695 (—OH). <sup>1</sup>H NMR (500 MHz)  $\delta_H$  7.44 (d,  $J$  = 6.1 Hz, 1H), 7.25 (d,  $J$  = 10.2 Hz, 1H), 7.12 (d,  $J$  = 7.4 Hz, 1H), 7.06–7.02 (m, 2H), 6.88 (d,  $J$  = 5.4 Hz, 1H), 6.49 (dd,  $J$  = 8.1, 1.4 Hz, 1H), 6.44 (s, 1H), 4.98 (s, 2H), 4.34 (s, 1H), 4.19 (s, 3H). <sup>13</sup>C NMR (126 MHz)  $\delta_C$  167.76, 159.33, 159.07, 154.72, 149.57, 148.50, 136.38, 129.77, 122.29, 114.91, 110.13, 109.09, 105.16, 104.06, 57.59. LC/MS (ESI,  $m/z$ ): 327 [M + H]<sup>+</sup>. HPLC purity: 96.24 %, retention time: 3.42 min.

**5.1.1.2.23. 2-Methoxy-4-(2-(5-(*m*-tolyl)-1,3,4-oxadiazol-2-yl)vinyl)phenol (6g)**

White solid, yield 89%; mp 117–119 °C; TLC (DCM/Methanol 90:10 v/v);  $R_f$  = 0.75. FT-IR ( $\nu$  cm<sup>-1</sup>): 3664 (—OH). <sup>1</sup>H NMR (500 MHz)  $\delta_H$  7.48 (t,  $J$  = 1.4 Hz, 1H), 7.44 (t,  $J$  = 7.3, 1.2 Hz, 1H), 7.36 (t,  $J$  = 7.4 Hz, 2H), 7.23 (d,  $J$  = 8.6 Hz, 1H), 6.81–6.77 (m, 3H), 6.68 (d,  $J$  = 4.6 Hz, 1H), 4.36 (s, 1H), 4.10 (s, 3H), 2.21 (s, 3H). <sup>13</sup>C NMR (126 MHz)  $\delta_C$  165.25, 164.14, 149.10, 148.15, 138.98, 137.82, 131.01, 127.89, 126.70, 126.51, 123.18, 115.81, 110.58, 54.94, 20.85. LC/MS (ESI,  $m/z$ ): 309 [M + H]<sup>+</sup>. HPLC purity: 95.38%, retention time: 2.22 min.

**5.1.1.2.24. 2-Methoxy-4-(2-(5-(*p*-tolyl)-1,3,4-oxadiazol-2-yl)vinyl)phenol (6h)**

White solid, yield 84%; mp 110–112 °C; TLC (DCM/Methanol 90:10 v/v);  $R_f$  = 0.74. FT-IR ( $\nu$  cm<sup>-1</sup>): 3690 (—OH). <sup>1</sup>H NMR (500 MHz)  $\delta_H$  7.20 (s, 2H), 7.13 (d,  $J$  = 5.4 Hz, 2H), 7.09 (d,  $J$  = 10.3 Hz, 1H), 6.86 (d,  $J$  = 6.6 Hz, 1H), 6.72–6.68 (m, 2H), 6.58 (d,  $J$  = 1.2 Hz), 4.20 (s, 1H), 4.01 (s, 3H), 2.24 (s, 3H). <sup>13</sup>C NMR (126 MHz)  $\delta_C$  165.21, 163.88, 149.57, 148.50, 140.60, 137.52, 129.09, 126.98, 125.47, 116.18, 110.81, 54.28,

20.82. LC/MS (ESI,  $m/z$ ): 309  $[M + H]^+$ . HPLC purity: 97.43%, retention time: 4.74 min.

**5.1.1.2.25. 2-Methoxy-4-(2-(5-(4-nitrophenyl)-1,3,4-oxadiazol-2-yl)vinyl)phenol (6i)**

White solid, yield 87%; mp 125–127 °C; TLC (DCM/Methanol 90:10 v/v);  $R_f = 0.69$ . FT-IR ( $\nu$   $\text{cm}^{-1}$ ): 3698 (—OH).  $^1\text{H}$  NMR (500 MHz)  $\delta_{\text{H}}$  8.29 (d,  $J = 7.2$  Hz, 2H), 7.82 (d,  $J = 4.2$  Hz, 2H), 7.17 (d,  $J = 9.4$  Hz, 1H), 6.88 (d,  $J = 6.2$  Hz, 1H), 6.82–6.78 (m, 2H), 6.60 (d,  $J = 1.8$  Hz, 1H), 4.36 (s, 1H), 4.12 (s, 3H).  $^{13}\text{C}$  NMR (126 MHz)  $\delta_{\text{C}}$  168.60, 161.78, 150.68, 149.03, 147.39, 137.82, 132.07, 127.52, 124.68, 123.18, 115.81, 110.13, 59.48. LC/MS (ESI,  $m/z$ ): 340  $[M + H]^+$ . HPLC purity: 96.39%, retention time: 3.16 min.

**5.1.1.2.26. 2-Methoxy-4-(2-(5-(4-(trifluoromethyl)phenyl)-1,3,4-oxadiazol-2-yl)vinyl)phenol (6j)**

White solid, yield 82%; mp 111–113 °C; TLC (DCM/Methanol 90:10 v/v);  $R_f = 0.64$ . FT-IR ( $\nu$   $\text{cm}^{-1}$ ): 3740 (—OH).  $^1\text{H}$  NMR (500 MHz)  $\delta_{\text{H}}$  7.62 (d,  $J = 4.5$  Hz, 2H), 7.52 (d,  $J = 3.2$  Hz, 2H), 7.12 (d,  $J = 12.8$  Hz, 1H), 6.91 (d,  $J = 6.6$  Hz, 1H), 6.81–6.78 (m, 2H), 6.68 (d,  $J = 1.3$  Hz, 1H), 3.95 (s, 1H), 3.82 (s, 3H).  $^{13}\text{C}$  NMR (126 MHz)  $\delta_{\text{C}}$  167.22, 162.67, 150.51, 149.54, 136.41, 132.39 (q,  $J_{\text{C-F}} = 30.5$  Hz), 131.13, 127.53, 126.07 (q,  $J_{\text{C-F}} = 10.2$  Hz), 124.95, 123.21 (q,  $J_{\text{C-F}} = 264.2$  Hz), 115.81, 110.70, 57.46. LC/MS (ESI,  $m/z$ ): 363  $[M + H]^+$ . HPLC purity: 99.48%, retention time: 3.74 min.

**5.1.1.2.27. 2-Methoxy-4-(2-(5-(4-(trifluoromethoxy)phenyl)-1,3,4-oxadiazol-2-yl)vinyl)phenol (6k)**

White solid, yield 89%; mp 119–121 °C; TLC (DCM/Methanol 90:10 v/v);  $R_f = 0.78$ . FT-IR ( $\nu$   $\text{cm}^{-1}$ ): 3758 (—OH).  $^1\text{H}$  NMR (500 MHz)  $\delta_{\text{H}}$  7.55 (d,  $J = 4.8$  Hz, 2H), 7.10–7.06 (m, 3H), 6.87 (d,  $J = 6.3$  Hz, 1H), 6.80–6.78 (m, 2H), 6.68 (d,  $J = 7.3$  Hz, 1H), 3.94 (s, 1H), 3.82 (s, 3H).  $^{13}\text{C}$  NMR (126 MHz)  $\delta_{\text{C}}$  167.22, 162.28, 152.96, 148.10,

138.60, 127.03, 126.65, 125.03, 123.66, 123.18, 120.76 (q,  $J_{C-F} = 248.9$  Hz), 115.81, 110.96, 57.33. LC/MS (ESI,  $m/z$ ): 379  $[M + H]^+$ . HPLC purity: 97.13%, retention time: 3.92 min.

**5.1.1.2.28. 4-(2-(5-(4-Chlorophenyl)-1,3,4-oxadiazol-2-yl)vinyl)-2-methoxyphenol (6l)**

White solid, yield 80%; mp 104–106 °C; TLC (DCM/Methanol 90:10 v/v);  $R_f = 0.78$ . FT-IR ( $\nu$   $\text{cm}^{-1}$ ): 3710 (—OH).  $^1\text{H}$  NMR (500 MHz)  $\delta_{\text{H}}$  7.50 (d,  $J = 4.3$  Hz, 2H), 7.43 (d,  $J = 7.1$  Hz, 2H), 7.09 (d,  $J = 5.2$  Hz, 1H), 6.86 (d,  $J = 8.5$  Hz, 1H), 6.81–6.77 (m, 2H), 6.68 (d,  $J = 7.3$  Hz, 1H), 3.94 (s, 1H), 3.82 (s, 3H).  $^{13}\text{C}$  NMR (126 MHz)  $\delta_{\text{C}}$  166.46, 162.26, 150.85, 148.16, 137.22, 129.45, 128.39, 128.09, 127.58, 123.18, 115.81, 110.25, 57.39. LC/MS (ESI,  $m/z$ ): 329  $[M + H]^+$ . HPLC purity: 98.19%, retention time: 2.20 min.

**5.1.1.2.29. 4-(2-(5-(2,4-Dichlorophenyl)-1,3,4-oxadiazol-2-yl)vinyl)-2-methoxyphenol (6m)**

White solid, yield 84%; mp 126–128 °C; TLC (DCM/Methanol 90:10 v/v);  $R_f = 0.75$ . FT-IR ( $\nu$   $\text{cm}^{-1}$ ): 3740 (—OH).  $^1\text{H}$  NMR (500 MHz)  $\delta_{\text{H}}$  7.82 (d,  $J = 1.4$  Hz, 1H), 7.54 d,  $J = 7.5$  Hz, 1H), 7.32 (dd,  $J = 6.4, 1.4$  Hz, 1H), 7.16 (d,  $J = 5.0$  Hz, 1H), 6.93 (d,  $J = 9.2$  Hz, 1H), 6.81–6.77 (m, 2H), 6.68 (d,  $J = 7.4$  Hz, 1H), 4.13 (s, 1H), 3.96 (s, 3H).  $^{13}\text{C}$  NMR (126 MHz)  $\delta_{\text{C}}$  166.84, 154.33, 149.84, 148.08, 137.74, 135.01, 134.93, 131.72, 128.50, 127.05, 123.71, 115.26, 110.41, 57.28. LC/MS (ESI,  $m/z$ ): 363  $[M + H]^+$ . HPLC purity: 96.10%, retention time: 3.41 min.

**5.1.1.2.30. 4-(2-(5-(4-Fluorophenyl)-1,3,4-oxadiazol-2-yl)vinyl)-2-methoxyphenol (6n)**

White solid, yield 77%; mp 127–129 °C; TLC (DCM/Methanol 90:10 v/v);  $R_f = 0.71$ . FT-IR ( $\nu$   $\text{cm}^{-1}$ ): 3714 (—OH).  $^1\text{H}$  NMR (500 MHz)  $\delta_{\text{H}}$  7.57–7.52 (m, 2H), 7.15 (t,  $J = 7.8$  Hz, 2H), 7.08 (d,  $J = 6.4$  Hz, 1H), 6.87 (d,  $J = 9.2$  Hz, 1H), 6.81–6.77 (m, 2H), 6.68

(d,  $J = 7.2$  Hz, 1H), 4.35 (s, 1H), 4.10 (s, 3H).  $^{13}\text{C}$  NMR (126 MHz)  $\delta_{\text{C}}$  166.81, 165.16 (d,  $J_{\text{C-F}} = 225.3$  Hz), 163.80), 149.45, 148.41, 137.17, 129.09 (d,  $J_{\text{C-F}} = 3.8$  Hz), 127.58 (d,  $J_{\text{C-F}} = 10.6$  Hz), 123.55, 123.04, 116.41, 115.81 (d,  $J_{\text{C-F}} = 15.2$  Hz), 110.71, 57.95. LC/MS (ESI,  $m/z$ ): 313  $[\text{M} + \text{H}]^+$ . HPLC purity: 95.80%, retention time: 6.25 min.

**5.1.1.2.31. 4-(2-(5-(2,4-Difluorophenyl)-1,3,4-oxadiazol-2-yl)vinyl)-2-methoxyphenol (6o)**

White solid, yield 78%; mp 119–121 °C; TLC (DCM/Methanol 90:10 v/v);  $R_f = 0.79$ . FT-IR ( $\nu \text{ cm}^{-1}$ ): 3749 (—OH).  $^1\text{H}$  NMR (500 MHz)  $\delta_{\text{H}}$  7.54 (t,  $J = 7.4, 5.0$  Hz, 1H), 7.12 (d,  $J = 4.2$  Hz, 1H), 6.93 (dd,  $J = 11.1, 2.1$  Hz, 3H), 6.79 (t,  $J = 2.6, 1.3$  Hz, 2H), 6.71 (d,  $J = 7.0$  Hz, 1H), 4.38 (s, 1H), 4.12 (s, 3H).  $^{13}\text{C}$  NMR (126 MHz)  $\delta_{\text{C}}$  167.05, 165.45 (d,  $J_{\text{C-F}} = 280.3$  Hz), 164.52 (d,  $J_{\text{C-F}} = 278.9$  Hz), 163.81, 162.45, 154.44, 149.57, 148.95, 137.42, 130.82 (d,  $J_{\text{C-F}} = 3.2$  Hz), 127.28 (d,  $J_{\text{C-F}} = 3.2$  Hz), 123.16, 115.62 (d,  $J_{\text{C-F}} = 4.2$  Hz), 114.52, 114.48, 113.21, 113.15 (d,  $J_{\text{C-F}} = 10.5$  Hz), 110.13, 105.00, 104.79 (d,  $J_{\text{C-F}} = 31.2$  Hz), 104.57, 57.17. LC/MS (ESI,  $m/z$ ): 331  $[\text{M} + \text{H}]^+$ . HPLC purity: 99.10%, retention time: 2.87 min.

**5.1.2 Biological evaluation**

**5.1.2.1 In-vitro studies**

**5.1.2.1.1 Cholinesterase (AChE and BChE) and BACE-1 inhibition assays**

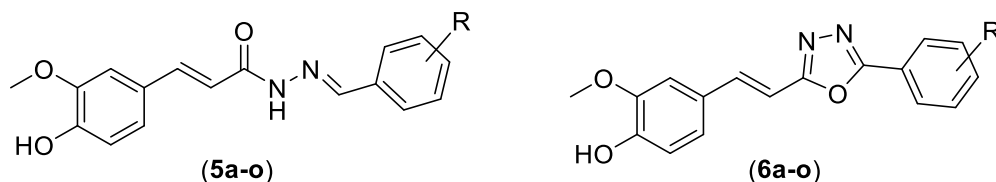
The cholinesterase inhibitory potential of synthesized target compounds (**5a–o**, and **6a–o**) was evaluated by Ellman colorimetric assay. The compounds displayed moderate to excellent inhibitory potential against both the cholinesterases (AChE and BChE). The Schiff bases (**5a–o**) showed moderately lower inhibitory potential compared to their cyclic oxadiazole counterparts (**6a–o**), respectively. The unsubstituted derivatives displayed moderate inhibition of AChE (**5a**,  $\text{IC}_{50} = 2.98 \mu\text{M}$ ; **6a**,  $\text{IC}_{50} = 2.14 \mu\text{M}$ ). The

substitution of electron-donating groups (EDGs) such as OCH<sub>3</sub> and CH<sub>3</sub> lead to reduced activity against AChE with inhibitory potential > 5 μM. The substitution of electron-withdrawing groups (EWGs) significantly improved the inhibitory potential of compounds. The Schiff bases with 4-OH, 2-OH and 4-NO<sub>2</sub> substitution showed moderate inhibition (**5d**, IC<sub>50</sub> = 1.09 μM; **5e**, IC<sub>50</sub> = 1.57 μM; **5i**, IC<sub>50</sub> = 1.04 μM), while their cyclic counterparts showed considerably higher inhibition of AChE (**6d**, IC<sub>50</sub> = 0.731 μM; **6e**, IC<sub>50</sub> = 0.865 μM; **6i**, IC<sub>50</sub> = 0.972 μM). All other EWGs (i.e. 2,4-diOH, 4-Cl, 2,4-diCl, 4-F, and 2,4-diF) substituted compounds showed excellent AChE inhibition. Among all the tested compounds, 4-CF<sub>3</sub> and 4-OCF<sub>3</sub> substitution exhibited excellent AChE inhibitory profile for Schiff bases (**5j**, IC<sub>50</sub> = 0.139 μM; **5k**, IC<sub>50</sub> = 0.419 μM), and their cyclic counterparts (**6j**, IC<sub>50</sub> = 0.068 μM; **6k**, IC<sub>50</sub> = 0.092 μM). Several findings suggested that inhibition of BChE is also a vital therapeutic strategy in the treatment of AD. The dual inhibition of AChE and BChE could be beneficial in halting the disease progression rather than providing symptomatic relief only [Greig et al. 2002, Greig et al. 2001]. Therefore, the BChE inhibitory potential of all the target compounds was also evaluated. The results of the BChE inhibition assay suggested that compounds **5b**, **5c**, **5g**, **5h**, **5i**, **5l**, **5m**, **5n**, **5o**, **6b**, **6c** and **6g** have mediocre inhibitory potential (> 10 μM). Several of the target compounds **5a**, **5d**, **5e**, **5f**, **5j**, **5k**, **6a**, **6d**, **6e**, **6f**, and **6h** exhibited micromolar inhibitory potential against BChE. Remaining compounds **6j**, **6k**, **6l**, **6m**, **6n**, and **6o** elicited excellent dual inhibitory potential against both cholinesterases (AChE and BChE).

In our quest to explore multifunctional therapeutic candidates, the FRET-based fluorometric BACE-1 inhibition assay was performed. The results of assay elicited that all the Schiff bases were poor BACE-1 inhibitors. Among the cyclic oxadiazoles, compounds **6a**, **6h**, **6i**, **6j**, **6k**, **6l**, **6m**, **6n**, and **6o** were excellent BACE-1 inhibitors. The

results of enzyme assays conferred that most of the tested compounds (**5f**, **5j**, **5k**, **5l**, **5m**, **5n**, **5o**, **6d**, **6e**, **6f**, **6i**, **6j**, **6k**, **6l**, **6m**, **6n** and **6o**) were excellent inhibitors of AChE, but only a few of them displayed significant and balanced inhibition against BChE and BACE-1. Compounds **6a** and **6h** showed superior inhibition of BACE-1 but were found to be devoid of activity against AChE or BChE ( $IC_{50} > 1 \mu M$ ). Interestingly, the compounds with dual cholinesterase inhibitory potential were observed to be good candidates in providing BACE-1 inhibition. Common multifunctional compounds (**6j**, **6k**, **6l**, **6m**, **6n**, and **6o**) with excellent and balanced inhibition of dual cholinesterase (AChE and BChE) and BACE-1 were selected as lead candidates for further experiments. The results of enzyme assays are summarized in Table 5.1.

**Table 5.1.** Cholinesterases (hAChE and hBChE) and hBACE-1 inhibition activity and selectivity index of compounds (Series I and II).



Comd.	R	$IC_{50} \pm SEM (\mu M)^a$			hAChE SI <sup>b</sup>	Log P <sup>d</sup>
		hAChE	hBChE	hBACE-1		
<b>5a</b>	-H	$2.98 \pm 0.066$	$5.89 \pm 0.039$	$6.40 \pm 0.10$	1.98	3.19
<b>5b</b>	2,3-diOCH <sub>3</sub>	>5	>10	nd	--	2.94
<b>5c</b>	3,4,5-triOCH <sub>3</sub>	>5	>10	nd	--	2.81
<b>5d</b>	4-OH	$1.09 \pm 0.015$	$2.14 \pm 0.042$	$4.68 \pm 0.152$	1.96	2.80
<b>5e</b>	2-OH	$1.57 \pm 0.021$	$2.89 \pm 0.031$	$2.63 \pm 0.084$	1.84	2.81
<b>5f</b>	2,4-diOH	$0.638 \pm 0.010$	$2.10 \pm 0.028$	$2.12 \pm 0.120$	3.07	2.41
<b>5g</b>	3-CH <sub>3</sub>	>5	>10	nd	--	3.68
<b>5h</b>	4-CH <sub>3</sub>	>5	>10	nd	--	2.99
<b>5i</b>	4-NO <sub>2</sub>	$1.04 \pm 0.026$	>10	$8.76 \pm 0.230$	--	3.54
<b>5j</b>	4-CF <sub>3</sub>	$0.139 \pm 0.009$	$2.36 \pm 0.062$	$7.15 \pm 0.127$	16.98	4.41
<b>5k</b>	4-OCF <sub>3</sub>	$0.419 \pm 0.018$	$3.86 \pm 0.052$	$8.42 \pm 0.154$	9.21	4.72
<b>5l</b>	4-Cl	$0.595 \pm 0.022$	>10	>10	--	3.75
<b>5m</b>	2,4-DiCl	$0.317 \pm 0.012$	>10	>10	--	4.31
<b>5n</b>	4-F	$0.407 \pm 0.015$	>10	$6.39 \pm 0.138$	--	3.35
<b>5o</b>	2,4-diF	$0.268 \pm 0.004$	>10	$5.27 \pm 0.195$	--	3.51



<b>6a</b>	-H	2.14 ± 0.029	3.12 ± 0.039	0.836 ± 0.103	1.45	3.54
<b>6b</b>	2,3-di OCH <sub>3</sub>	>5	>10	nd	--	3.29
<b>6c</b>	3,4,5-tri OCH <sub>3</sub>	>5	>10	nd	--	3.16
<b>6d</b>	4-OH	0.731 ± 0.021	1.94 ± 0.028	7.34 ± 0.096	2.65	3.17
<b>6e</b>	2-OH	0.865 ± 0.035	1.86 ± 0.040	6.78 ± 0.074	2.15	3.15
<b>6f</b>	2,4-diOH	0.279 ± 0.007	2.76 ± 0.026	8.12 ± 0.138	9.89	2.76
<b>6g</b>	3-CH <sub>3</sub>	>5	>10	nd		4.03
<b>6h</b>	4-CH <sub>3</sub>	4.32 ± 0.087	5.23 ± 0.076	0.649 ± 0.063	1.21	3.56
<b>6i</b>	4-NO <sub>2</sub>	0.972 ± 0.034	5.23 ± 0.076	4.56 ± 0.137	5.38	3.21
<b>6j</b>	4-CF <sub>3</sub>	0.068 ± 0.003	0.218 ± 0.014	0.255 ± 0.076	7.20	4.46
<b>6k</b>	4-OCF <sub>3</sub>	0.092 ± 0.008	0.163 ± 0.023	0.211 ± 0.091	1.77	4.48
<b>6l</b>	4-Cl	0.334 ± 0.018	0.736 ± 0.012	0.628 ± 0.062	2.20	4.10
<b>6m</b>	2,4-DiCl	0.220 ± 0.010	0.915 ± 0.049	0.864 ± 0.063	4.15	4.66
<b>6n</b>	4-F	0.284 ± 0.012	0.292 ± 0.076	0.479 ± 0.074	1.27	3.70
<b>6o</b>	2,4-diF	0.190 ± 0.004	0.420 ± 0.054	0.624 ± 0.031	2.21	3.86
	donepezil <sup>c</sup>	0.046 ± 0.003	1.94 ± 0.093	0.220 ± 0.006	42.2	
	rivastigmine <sup>c</sup>	2.58 ± 0.032	1.07 ± 0.054	nd	0.41	

<sup>a</sup>Data are represented as the mean IC<sub>50</sub> ± SEM of three separate experiments (n = 3). <sup>b</sup>Selectivity Ratio = IC<sub>50</sub> of hBChE/hAChE. <sup>c</sup>Ref. [Sharma et al. 2019b]. nd = not determined. <sup>d</sup>Log P value was determined using the shake flask method.

#### 5.1.2.1.2 Enzyme kinetics study

The enzyme kinetics study of most potential lead candidate **6j** was evaluated against AChE using six different concentrations of substrate, i.e., acetylthiocholine iodide (ATCI). Three different concentrations of compound **6j** were tested separately against each substrate concentration. The Lineweaver-Burk double reciprocal plot was drawn between the velocity of reaction (y-axis) and substrate concentrations (x-axis). The plots revealed decreased V<sub>max</sub>, while K<sub>m</sub> increased with increasing the concentration of test compound **6j**, which suggested the mixed type of AChE inhibition (Figure 5.1). In Lineweaver-Burk plot, the lines intersection point was at less than zero at x-axis and greater than zero at the y-axis, which indicated that ligand preferentially binds to free enzyme rather than enzyme-substrate complex. Further, Dixon plot was constructed between the slopes of Lineweaver-Burk plots and the concentration of test compound **6j**

(Figure 5.2). The intersection point at the x-axis of the plot can be considered as dissociation constant  $K_i$ , which was found to be  $0.043 \mu\text{M}$ .

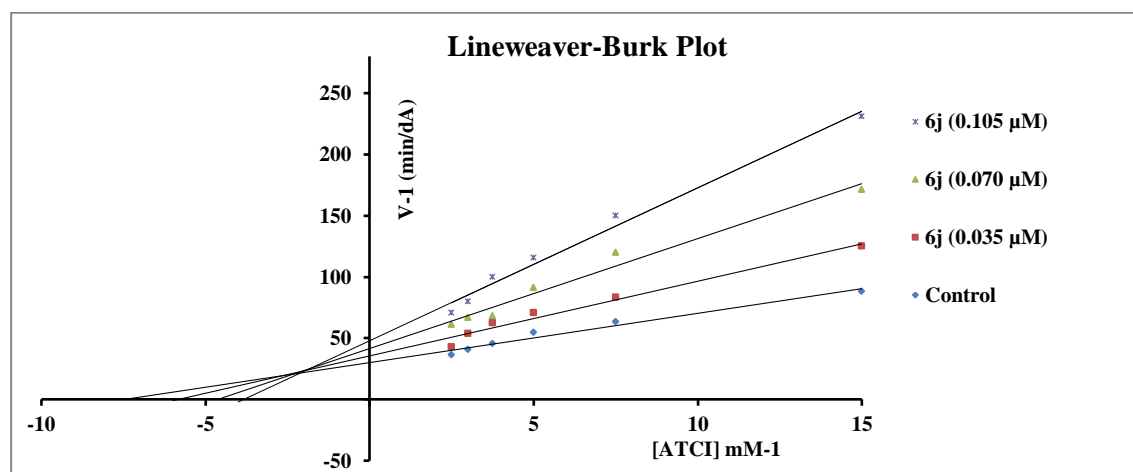


**Figure 5.1.** Lineweaver-Burk plot for the kinetic study of hAChE inhibition by compound **6j**.

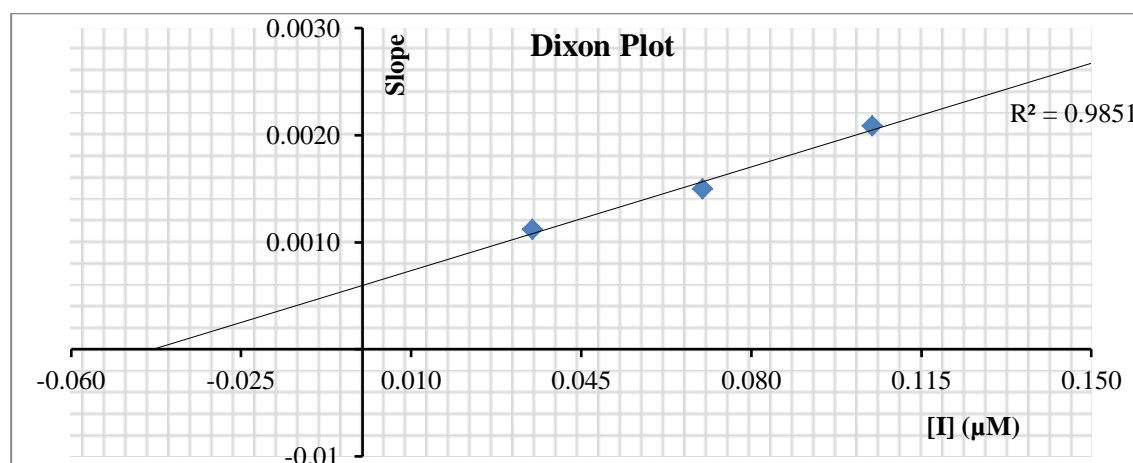


**Figure 5.2.** Dixon plot of compound **6j** at three different concentrations (0.035, 0.070, and 0.105  $\mu\text{M}$ ) showing  $K_i$  value of inhibitor as the negative intersection at the x-axis.

### 5.1.2.1.3 Propidium iodide displacement assay

The results of the enzyme kinetics study suggested a mixed type of enzyme inhibition by compound **6j**, which indicated its binding to both catalytic (CAS) and peripheral (PAS) anionic sites. The PAS-AChE is also reported to be the center of  $A\beta$  plaque formation and binding of compounds to this site might lead to anti- $A\beta$  aggregatory activity [López-Iglesias et al. 2014]. Therefore, the PAS-AChE binding potential of compounds was evaluated by propidium iodide displacement assay. The propidium

iodide is a known ligand bind specifically to PAS-AChE and responsible for increasing the fluorescence intensity up to 8-10 folds [Silva et al. 2013]. The results of assay indicated lower propidium iodide displacement capability by compounds **6l**, **6m**, **6n**, and **6o** while compounds **6j** and **6k** exhibited significantly higher displacement of propidium iodide, compared to donepezil at 10 and 50  $\mu\text{M}$  concentrations. These results signified the consensual binding of compounds **6j** and **6k** at PAS-AChE (Table 5.2).

**Table 5.2.** Propidium iodide displacement and predicted BBB permeability.

Compd.	Propidium iodide displacement from AChE PAS (% inhibition) <sup>a</sup>		PAMPA-BBB permeability	
	At 10 $\mu\text{M}$	At 50 $\mu\text{M}$	$P_{e(\text{exp})}$ ( $10^{-6} \text{ cm.s}^{-1}$ )	Prediction
<b>6j</b>	32.94 $\pm$ 1.09	50.74 $\pm$ 1.74	5.3 $\pm$ 0.29	CNS+ <sup>b</sup>
<b>6k</b>	26.68 $\pm$ 1.41	42.25 $\pm$ 1.65	6.2 $\pm$ 0.24	CNS+ <sup>b</sup>
<b>6l</b>	14.63 $\pm$ 1.82	22.63 $\pm$ 1.084	3.9 $\pm$ 0.18	CNS $\pm$ <sup>c</sup>
<b>6m</b>	12.85 $\pm$ 1.26	16.41 $\pm$ 1.07	7.1 $\pm$ 0.30	CNS+ <sup>b</sup>
<b>6n</b>	15.49 $\pm$ 1.13	20.85 $\pm$ 1.58	4.3 $\pm$ 0.22	CNS $\pm$ <sup>c</sup>
<b>6o</b>	11.38 $\pm$ 1.26	14.65 $\pm$ 1.65	6.7 $\pm$ 0.32	CNS+ <sup>b</sup>
donepezil	22.14 $\pm$ 1.50	31.52 $\pm$ 1.29	6.4 $\pm$ 0.20	CNS+ <sup>b</sup>

<sup>a</sup>The propidium iodide displacement assay was performed at 10  $\mu\text{M}$  and 50  $\mu\text{M}$  concentrations of respective inhibitors. <sup>b</sup>CNS+’ suggested excellent ( $P_e > 4.4 \times 10^{-6} \text{ cm s}^{-1}$ ) and <sup>c</sup>‘CNS $\pm$ ’ suggested uncertain ( $4.4$  to  $1.8 \times 10^{-6} \text{ cm s}^{-1}$ ) brain permeability values. Data are expressed as the mean  $\pm$  SEM of three separate experiments ( $n = 3$ ).

#### 5.1.2.1.4 Parallel artificial membrane permeation assay (PAMPA-BBB)

The BBB permeability is the prerequisite requirement for the compounds targeted for CNS delivery [Kumar et al. 2018]. The PAMPA assay was performed to predict the BBB permeability characteristics of test compounds. Initially, the experiment was validated by comparing the experimental ( $P_{e(\text{exp})}$ ) and reference ( $P_{e(\text{ref})}$ ) permeability values of nine commercial drugs, to determine the range of permeability values for excellent, uncertain and poor permeability values as per our previously prescribed protocols [Seth et al. 2018, Sharma et al. 2019a]. The results of the PAMPA assay are summarized in Table 5.2. Compounds **6j**, **6k**, **6m**, and **6o** exhibited appreciable BBB permeability, while **6l** and **6n** showed uncertain permeability predictions.

These results suggested that compounds **6j** and **6k** exhibited balanced inhibition of both cholinesterases (hAChE and hBChE) and hBACE-1. These compounds also have commendable propidium iodide displacement capability, along with the considerable BBB permeability. Therefore, compounds **6j** and **6k** were selected as lead candidates for further pharmacological investigations.

#### ***5.1.2.1.5 Self- and AChE-induced A $\beta$ aggregation inhibition by thioflavin T assay***

Amyloid plaque formation and its accumulation in neuronal cells lead to loss of cognitive functions in AD [Lemkul and Bevan 2012]. The results of the propidium iodide displacement assay advocated that the compounds **6j** and **6k** have the potential to reduce the levels of AChE and prevent the overproduction of A $\beta$  [Inestrosa et al. 1996]. Therefore, thioflavin-T assay was performed to determine the self- and AChE-induced anti-A $\beta$  aggregation potential of compounds **6j** and **6k**. The experiment was conducted at three different concentration ratios of A $\beta$  and inhibitor (10:5  $\mu$ M, 10:10  $\mu$ M, and 10:20  $\mu$ M, respectively). The results were reported as normalized fluorescence intensity (NFI, Figures 5.3A and 5.3B) and % A $\beta$  aggregation inhibition (Figures 5.4A and 5.4B). The results showed increased A $\beta$  inhibitory potential with an increasing concentration of inhibitor. The results revealed that the inhibitory potential of compound **6j** (self-induced: 24–66%; hAChE-induced: 49–83%) and **6k** (self-induced: 22–49%; hAChE-induced: 32–76%) were comparatively higher than donepezil (self-induced: 22–36%; hAChE-induced: 26–73%). In AChE-induced experiment, similar to donepezil, compounds **6j** and **6k** have significantly higher anti-A $\beta$  aggregation potential compared to self-induced experiment.

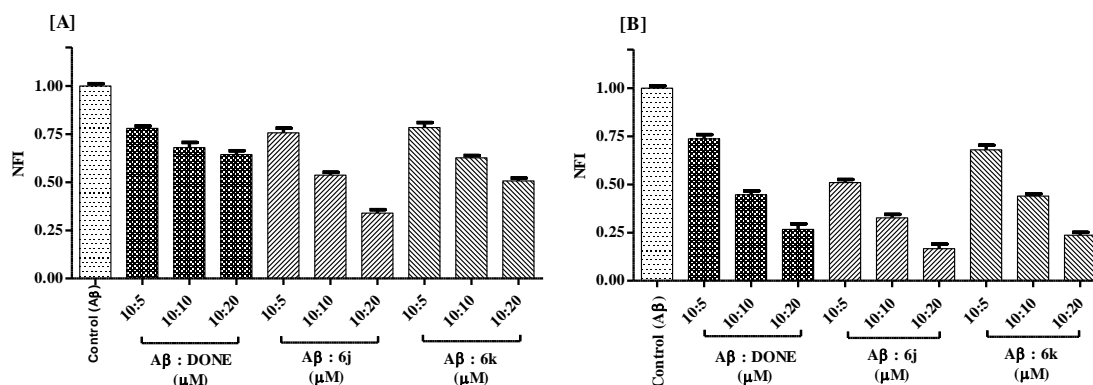


**Figure 5.3** Results of thioflavin T assay for compounds **6j** and **6k** in [A] self-induced; [B] AChE-induced experiments. Each bar displays the values of normalized fluorescence intensity (NFI) as the mean  $\pm$  SEM of three separate experiments ( $n = 3$ ).

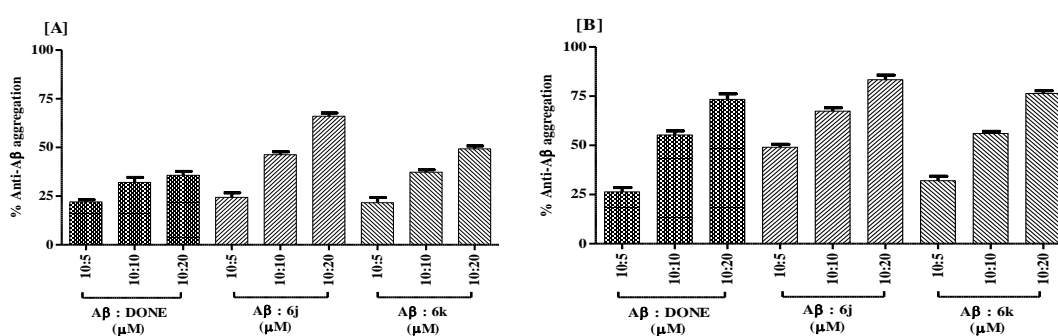


**Figure 5.4** The results of % anti-A $\beta$  aggregation activity in thioflavin T assay. Data are expressed as the mean  $\pm$  SEM of three separate experiments ( $n = 3$ ).

#### 5.1.2.1.6 Neuroprotection studies on SH-SY5Y cell line

Neuroprotective activity of compounds **6j** and **6k** was determined against human neuroblastoma SH-SY5Y cell lines by 3-(4,5-dimethylthiazol-2-yl)-2,5-diphenyl tetrazolium bromide (MTT) assay [More and Vince 2012]. The activity was performed using four different concentrations (10, 20, 40, and 80  $\mu$ M) of test compounds to determine their potential in preventing cell death against A $\beta$ -induced oxidative stress. In this assay, 20  $\mu$ M of A $\beta$  was incubated with SH-SY5Y cells, which attenuated the % cell viability to 61% compared to control. The incubation of A $\beta$  and SH-SY5Y cells in the presence of test compounds **6j** (70.45–89.61%) and **6k** (65.11–80.27%) lead to significantly augmented % cell viabilities. Overall results suggested the neuroprotective

activity of compounds **6j** and **6k** towards SH-SY5Y neuroblastoma cell lines against A $\beta$ -induced oxidative stress.

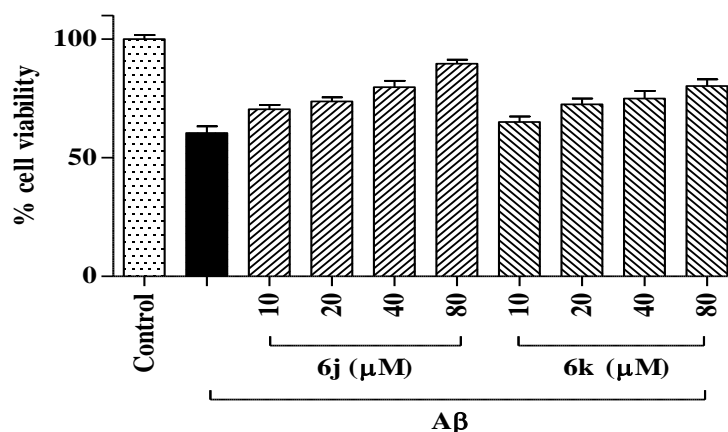


**Figure 5.5** Neuroprotective activity of compounds **6j** and **6k** against A $\beta$ -induced oxidative stress in SH-SY5Y cell lines by MTT assay. Each bar displays the values of % cell viability as the mean  $\pm$  SEM of three separate experiments (n = 3).

### 5.1.2.2 *In-vivo* behavioral studies

#### 5.1.2.2.1 Acute oral toxicity study

The acute oral toxicity study was performed as per OECD guidelines 425 on healthy female Wistar rats. The results showed no adverse effects of **6j** and **6k** up to 677, 1333, 2000 mg/kg concentration. The results suggested a significant margin of safety of compounds **6j** and **6k** to be processed further for *in-vivo* investigations.

#### 5.1.2.2.2 Scopolamine-induced amnesia model: Y-maze test

The efficacy of potential leads **6j** and **6k** was evaluated in ameliorating cognitive dysfunctions by the Y maze test in healthy Wistar rats. Scopolamine acts by increasing the cholinergic deficit and was used to induce the impairment of learning and memory [Klinkenberg and Blokland 2010]. The compounds were evaluated at three graded doses (2.5, 5, and 10 mg/kg, p.o.) to understand the dose-response effects, and the results were compared with donepezil (5 mg/kg, p.o.) as the reference standard.

The experiment involved the administration of test/standard for seven consecutive days.

On the seventh day, scopolamine was administered (0.5 mg/kg, i.p.) to induce the

learning and memory impairment followed by the Y maze test to assess the improvement in learning and memory behavior in rats. The results were calculated in the form of percentage spontaneous alternations, the increase of which can be considered as a score of amelioration in cognitive dysfunctions.

The results of the Y maze test elicited impairment in learning and memory with the administration of scopolamine as its percentage spontaneous alternation score decreased significantly ( $^{***}p < 0.001$ , Figure 5.6A) compared to control. The significant ( $^{###}p < 0.001$ , Figure 5.6A) improvement in learning and memory behavior observed with the administration of standard donepezil (5 mg/kg) compared to the scopolamine group. The treatment by compounds **6j** and **6k** demonstrated dose-dependent amelioration in cognitive dysfunctions. The treatment with compound **6j** exhibited significant improvement ( $^{###}p < 0.001$ , Figure 5.6A) in learning and memory behavior at all three tested doses compared to control, while compound **6k** showed the same response at two higher doses only, i.e., 5 and 10 mg/kg. Interestingly, compound **6j** (5 and 10 mg/kg) and **6k** (10 mg/kg) elicited comparable (ns = nonsignificant, Figure 5.6A) efficacy with donepezil (5 mg/kg) in ameliorating cognitive deficit. Further, similar scores of total arm entries amongst all the groups confirmed that scopolamine or any other treatment did not hamper the motor activity in rats during the test (ns = nonsignificant, Figure 5.6B).

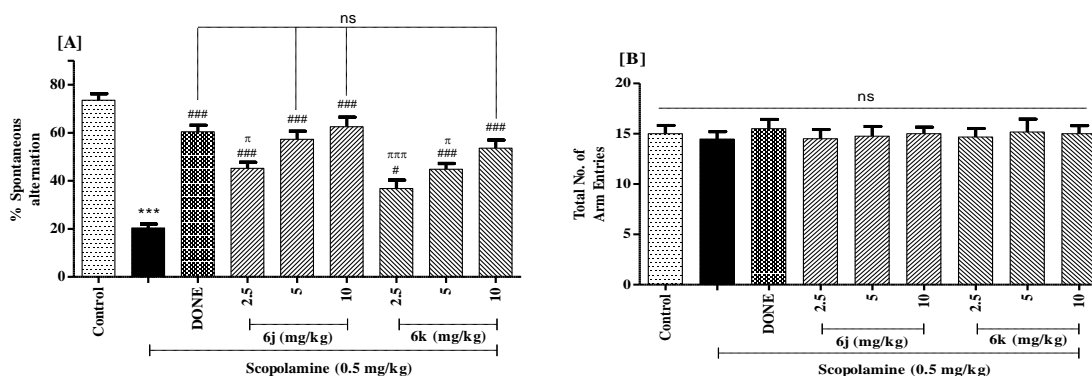


**Figure 5.6** The effect of compounds **6j** and **6k** on scopolamine-induced amnesia model

by Y maze test in rats. [A] Percentage spontaneous alterations and; [B] total arm entries. Data are expressed as the mean  $\pm$  SEM (n = 6). \*\*\* p < 0.001 versus control; ### p < 0.001, # p < 0.05 versus scopolamine;  $\pi\pi\pi$  p < 0.001,  $\pi$  p < 0.05 versus donepezil (DONE); ns = non-significant.

#### 5.1.2.2.3 A $\beta$ -induced AD phenotypic model: Morris water maze test

The production and deposition of A $\beta$  plaques are one of the most crucial factors involved in AD. The results of *in-vitro* assays indicated that compound **6j** was the most potent inhibitor of A $\beta$  aggregation; thereby, *in-vivo* investigation was conducted by intracerebrovascular (ICV) administration of A $\beta$  through stereotaxic surgery in rats. The ICV rat model is a well-known model producing an AD-like phenotypic condition. For this study, the rats were divided into four groups of six animals each: sham (healthy control), model (A $\beta$  group), standard (donepezil, 5 mg/kg), and test (**6j**, 10 mg/kg). After the stereotaxic surgery, all the groups were administered A $\beta$  (4  $\mu$ M, 5  $\mu$ l) through stereotaxic surgery except the sham group of animals, which were administered saline only. Following the recovery period of seven days, the treatment of respective groups of animals was given to consecutive nine days. During the last five days of treatment, the Morris water maze test was performed to measure the escape latency time (ELT) and total platform crossovers for 90 s.

The results of the Morris water maze test demonstrated impairment in learning and memory by a model group of animals with a significant prolongation of ELT (Figure 5.7A), while total platform crossovers were reduced considerably (Figure 5.7B) compared to sham group of animals. The treatment by **6j** and donepezil exhibited a remarkable reduction in ELT (Figure 5.7A), while total platform crossovers increased significantly (Figure 5.7B) compared to the model group. The results also signified that compound **6j** has a slightly better effect in ameliorating cognitive dysfunction compared to donepezil at the tested doses, which might be attributed to superior multifunctional activities.



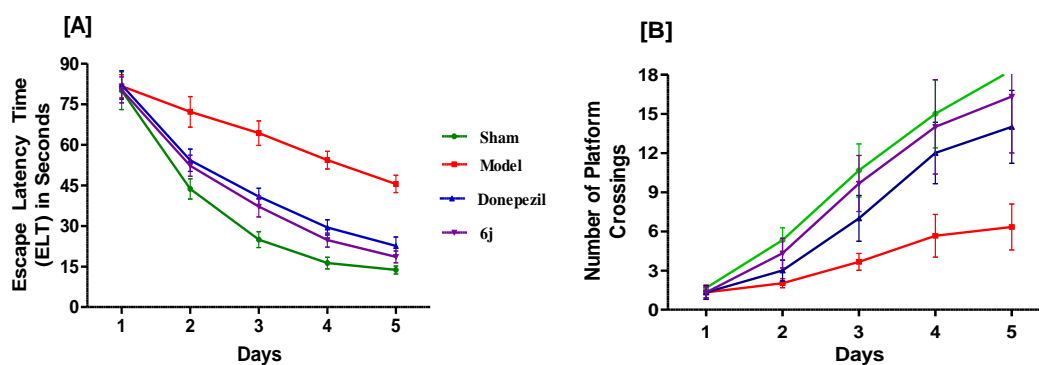


**Figure 5.7** Assessment of improvement in learning and memory impairment by compound **6j** in Morris water maze test; (A) escape latency time (ELT); (B) numbers of platform crossings. Data are expressed as the mean  $\pm$  SEM ( $n = 6$ )

#### 5.1.2.3 *Ex-vivo* study

Following the Y maze test, hippocampal regions of rat brains were isolated and homogenized. The *ex-vivo* study was performed to analyze AChE levels and oxidative stress biomarkers by treatment with **6j** (10 mg/kg), **6k** (10 mg/kg), and donepezil (5 mg/kg) in hippocampal brain homogenates.

The AChE level in hippocampal brain homogenates was estimated in terms of rate of substrate hydrolyzed by Ellman colorimetric assay. The administration of scopolamine significantly elevated ( $p < 0.001$ , Figure 5.8 A) AChE activity compared to the control group. The treatment by compounds (test/standard) significantly attenuated the AChE activity by lowering the rate of substrate hydrolysis ( $p < 0.001$ , Figure 5.8A) compared to the scopolamine group. Moreover, **6j** attenuated AChE activity comparable (ns = nonsignificant, Figure 5.8A) to donepezil.

The scopolamine is reported to cause oxidative stress, and therefore, the antioxidant activity of compounds **6j** and **6k** was evaluated by estimating the levels of important oxidative stress biomarkers such as malonaldehyde (MDA) and superoxide dismutase (SOD) in hippocampal brain homogenates. The increased levels of MDA and attenuation of SOD are indicators of oxidative stress induction. The MDA is generated as a byproduct of lipid peroxidation reaction [Placer et al. 1966], while SOD responsible

for specific dismutation of superoxide radicals into free oxygen [McCord and Fridovich 1969].

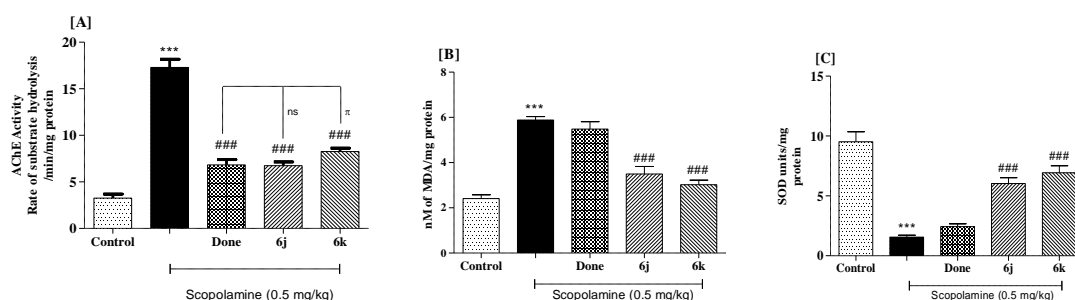


**Figure 5.8** *Ex-vivo* study of compounds **6j** and **6k** to assess the levels of; [A] AChE; [B] MDA and; [C] SOD. Data are expressed as the mean  $\pm$  SEM (n = 6). \*\*\* p < 0.001 versus control; ### p < 0.001 versus scopolamine; π p < 0.05, ns = nonsignificant versus donepezil (Done).

The results of the *ex-vivo* study demonstrated that scopolamine administration is responsible for inducing oxidative stress by significantly increasing the levels of MDA (\*\*p < 0.001, Figure 5.8B) and considerably lowering the levels of SOD (\*\*p < 0.001, Figure 5.8C) compared to control. The treatment by compound **6j** and **6k** showed remarkable attenuation in levels of MDA (###p < 0.001, Figure 5.8B), while the levels of SOD were observed to be significantly higher (###p < 0.001, Figure 5.8C) compared to scopolamine group. These results demonstrated the significant antioxidant potential of compounds **6j** and **6k**, while donepezil is devoid of antioxidant potential.

#### 5.1.2.4 Pharmacokinetic study

The most potent multifunctional lead candidate **6j** was evaluated for its pharmacokinetic parameters following an oral administration in male Wistar rats at the dose of 10 mg/kg, p.o. The plasma drug concentration was determined at different time points 0 (pre-dose), 0.5, 1, 2, 4, 8, 16, 24, 36, 48, 60, and 72 h to calculate pharmacokinetic parameters such as  $C_{max}$ ,  $T_{max}$ ,  $AUC_{0-24}$ ,  $t_{1/2}$  and mean residence time (MRT) were evaluated for pharmacokinetic profiling. The study was performed using the extravascular non-compartment model in Kinetica version 5.0 (Thermo Scientific

Kinetica, USA). The results are summarized in Table 5.3, which demonstrated that compound **6j** has appreciable oral absorption and bioavailability following an oral administration.

**Table 5.3.** Pharmacokinetic evaluation after an oral administration of **6j** (10 mg/kg, p.o.)

Parameters	Effect of <b>6j</b> *
$C_{\max}$ (ng/mL)	$50.4 \pm 2.3$
$T_{\max}$ (h)	$3.32 \pm 1.1$
$(AUC)_{0-24}$ (ng/mL*h)	$726 \pm 39$
$t_{1/2}$ (h)	$14.4 \pm 1.7$
MRT (h)	$20.7 \pm 1.2$

\*All values are expressed as mean  $\pm$  SEM (n = 3).

### 5.1.3 *In-silico* molecular docking study

The *in-silico* molecular docking study was performed to determine the consensual binding interactions of compound **6j** with the active sites of AChE (PDB ID: 4EY7) and BACE-1 (PDB ID: 2ZJM). Schrödinger Maestro 2018.4 platform with the Glide XP module was used to conduct the molecular docking experiments. Initially, the prepared protein grids and docking protocols were validated by extracting and re-docking the co-crystallized ligands (donepezil and F1M) into the respective proteins, i.e., AChE and BACE-1, respectively. The actual co-crystallized ligand was superimposed with the re-docked pose, and the RMSD value was calculated. The results showed the RMSD values of 0.3496 and 1.1903 for AChE and BACE-1 protein grids, respectively (Figures 5.9 and 5.10). The Glide XP visualized tool was used to visualize the docking images.

The results of the docking of **6j** on AChE demonstrated that the ferulic acid part of the molecule was inclined towards PAS, while 4-CF<sub>3</sub> substituted phenyl terminal was extended deep into the CAS. Compound **6j** interacted effectively with all the PAS residues through hydrophobic (Tyr72, Tyr124, Trp286, and Tyr341) and charged (Asp74) interactions. The extension of 4-CF<sub>3</sub> substituted phenyl terminal into the CAS

formed the polar interactions with Ser203 and His447. Additionally, the phenyl ring contacted with the imidazole nucleus of His447 through  $\pi$ - $\pi$  stacking interaction. Furthermore, this phenyl terminal ring and 1,3,4-oxadiazole formed the  $\pi$ - $\pi$  stacking interactions with the anionic subsite residues Trp86 and Phe338, respectively, and with Glu202 through charged interaction. Compound **6j** also interacted hydrophobically with Phe295 and Phe297 at acyl binding pocket and through glycine interactions with Gly120, Gly121, and Gly122 at oxyanion hole (Figures 5.11A and 5.11B).

Additionally, the binding pattern of **6j** was observed on BACE-1 protein, and the results are represented in Figures 5.12A and 5.12B. The results demonstrated charged interactions of aspartate dyads (Asp32 and Asp228) within the periphery of 5 Å distance from the molecule. The results also exhibited interactions of compound **6j** with several additional BACE-1 residues, which might be beneficial in holding the molecule within the active binding pocket. Overall results of molecular docking studies of **6j** showed consensual interactions with CAS and PAS residues of AChE and aspartate dyads of BACE-1, which were in complete agreement with *in-vitro* and *in-vivo* assays.

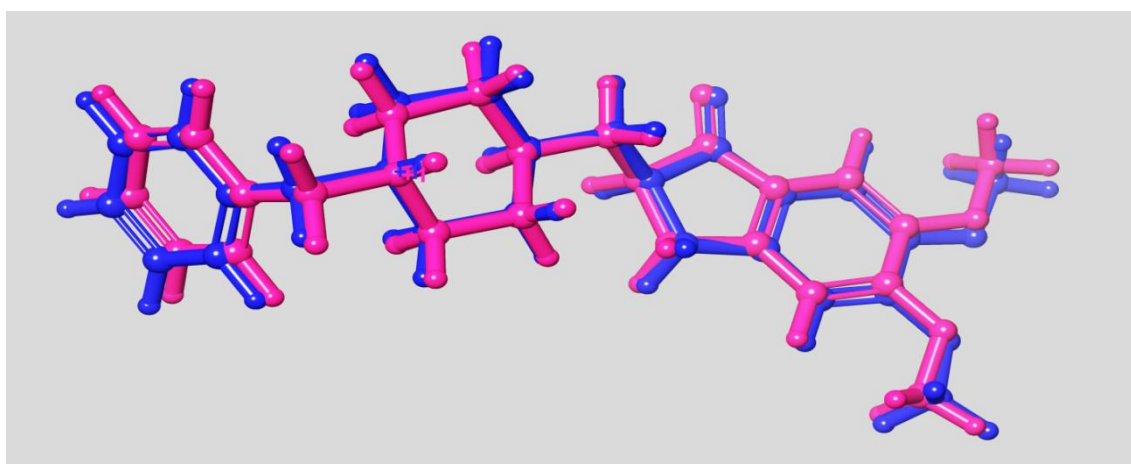


**Figure 5.9.** Validation experiment showing re-docked (pink) and co-crystallized (blue) poses of donepezil on 4EY7 (RMSD = 0.3496 Å).

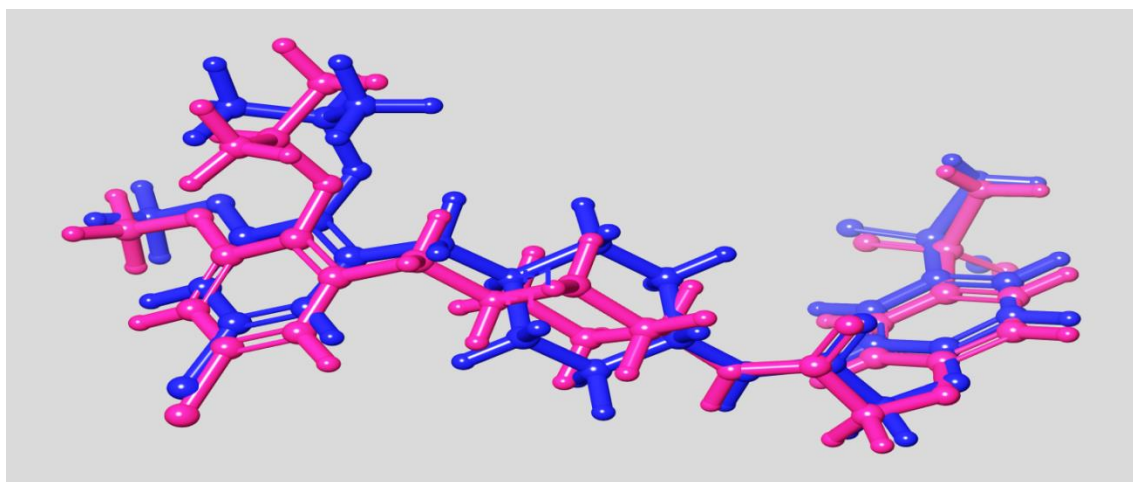


**Figure 5.10** Validation experiment showing re-docked (pink) and co-crystallized (blue) poses of F1M on 2ZJM (RMSD = 1.1903 Å).

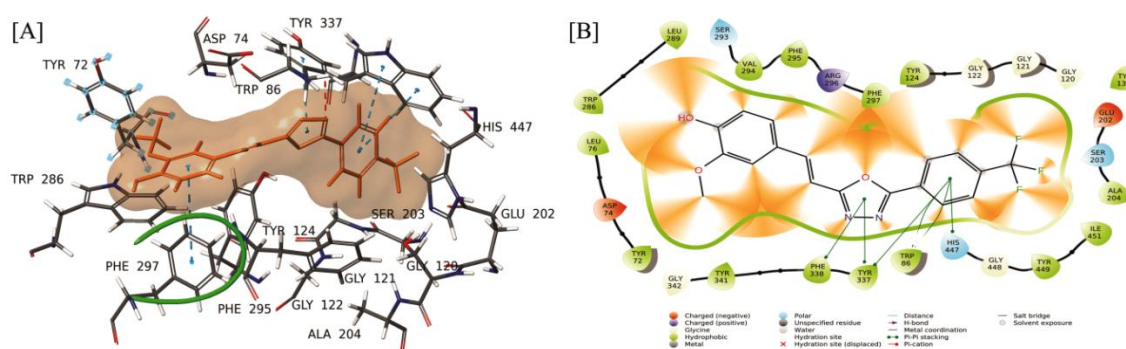


**Figure 5.11** The molecular docking study of **6j** on AChE. [A] 3D and [B] 2D docked poses.

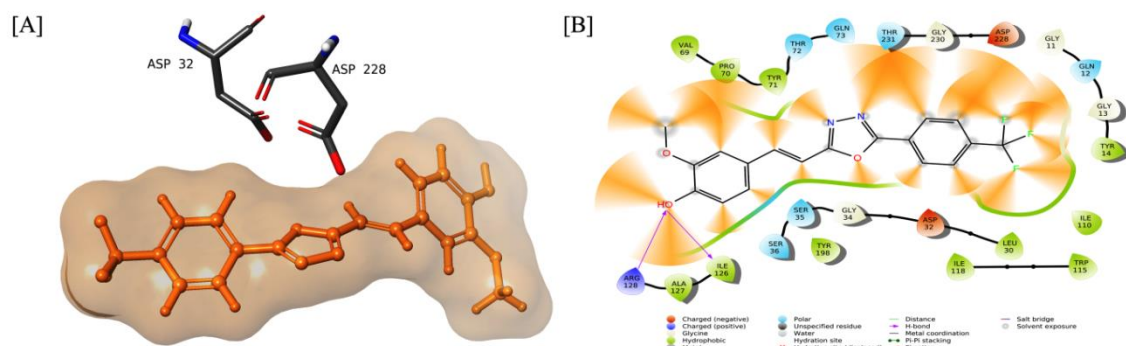


**Figure 5.12** The molecular docking study of **6j** on BACE-1. [A] 3D and [B] 2D docked poses.

## 5.2 PART-II: SERIES III AND IV

### 5.2.1 Chemistry

#### *5.2.1.1 Synthesis of Series III (12a–o): Pyridyl piperazine analogs with substituted N'-Benzylideneacetohydrazide; and Series IV (13a–o): Substituted 2-phenyl-1,3,4-oxadiazole tethered with Pyridyl piperazine*

The schematic representation of the synthesis of target molecules **12a–o** and **13a–o** was mentioned in Scheme 2- Experimental Section. Molecular hybrids of 2-pyridylpiperazine and substituted terminal phenyl groups with carbohydrazide imine (**12a–o**) and 1,3,4-oxadiazole (**13a–o**) linkers were prepared. Initially, the mixture of 2-pyridylpiperazine (**7**) and pyridine in DCM was added with phenyl chloroformate (**8**) dropwise at 0–5 °C. The reaction mixture was stirred for 2 h at room temperature to get the intermediate (**9**). Further intermediate (**9**) was refluxed with hydrazine hydrate in absolute ethanol for 6 h resulted in compound (**10**). The addition of respective aromatic aldehydes (**11a–o**) in the mixture of compound (**10**) in absolute ethanol with few drops of glacial acetic acid followed with refluxing the mixture for 6–8 h yielded corresponding carbohydrazide imines (**12a–o**). Subsequently, imines (**13a–o**) were stirred with chloramine T in absolute ethanol at room temperature for 30 min resulted in target oxadiazole hybrids (**13a–o**). The structures of all synthesized compounds were confirmed by spectroscopic studies (FT-IR, <sup>1</sup>H and <sup>13</sup>C NMR). The FT-IR spectra of carbohydrazide imines (**12a–o**) showed stretching bands of NH, C=O, and C=N in the range of 3265–3208, 1695–1652, and 1604–1571 cm<sup>-1</sup>, respectively. The cyclization of oxadiazole in compounds (**13a–o**) was confirmed by the absence of C=O band. The <sup>1</sup>H NMR spectra of compounds (**12a–o**) displayed distinguished signal for N=CH proton at  $\delta_{\text{H}} = 8.10\text{--}8.33$  ppm, and D<sub>2</sub>O exchanged signal in the proximity of  $\delta_{\text{H}} = 10.59\text{--}10.65$  ppm for NH proton. The oxadiazole formation in compounds (**13a–o**) was confirmed by

the disappearance of signals of N=CH and NH protons. Also, the  $^{13}\text{C}$  NMR spectra of compounds (**13a–o**) showed the appearance of characteristic signals in the range of  $\delta_{\text{C}} = 168.41\text{--}164.18$  and  $160.01\text{--}158.98$  ppm, respectively to confirm oxadiazole carbons. Further, the mass spectra of all the compounds confirmed the molecular weight of all the target compounds. The % purity of compounds was found to be  $\geq 95\%$  by HPLC.

### 5.2.1.2 Characterization of the synthesized compounds (Series III and IV)

#### 5.2.1.2.1 Phenyl 4-(pyridin-2-yl)piperazine-1-carboxylate (**9**).

Pale yellow solid, yield: 88%, Mp:  $115\text{--}117$  °C;  $R_{\text{f}} = 0.78$  (DCM:MeOH, 98:02 v/v); FT-IR (Alpha ATR,  $\nu$   $\text{cm}^{-1}$ ): 1664 (C=O).  $^1\text{H}$  NMR (500 MHz, DMSO- $d_6$ )  $\delta$ : 8.10 (s, 1H), 7.45 (s, 1H), 7.20–7.10 (m, 2H), 7.0–6.94 (m, 3H), 6.73 (d,  $J = 3.5$  Hz, 2H), 3.72–3.64 (dd,  $J = 33.5, 4.3$  Hz, 8H).  $^{13}\text{C}$  NMR (126 MHz, DMSO- $d_6$ )  $\delta$ : 158.90, 154.58, 150.94, 148.87, 140.12, 126.02, 113.61, 107.70, 47.62, 43.78.

#### 5.2.1.2.2 4-(Pyridin-2-yl)piperazine-1-carbohydrazide (**10**).

White solid, yield: 84%, Mp:  $108\text{--}110$  °C;  $R_{\text{f}} = 0.61$  (DCM:MeOH, 98:02 v/v); FT-IR (Alpha ATR,  $\nu$   $\text{cm}^{-1}$ ): 1665 (C=O).  $^1\text{H}$  NMR (500 MHz, DMSO- $d_6$ )  $\delta$ : 8.20 (s, 1H, —NH, D<sub>2</sub>O exchangeable), 7.40 (t,  $J = 4.6$  Hz, 1H), 6.62–6.54 (m, 2H), 5.10 (t,  $J = 7.2$  Hz, 1H), 4.3 (d,  $J = 6.0$  Hz 2H, —NH, D<sub>2</sub>O exchangeable), 3.70 (dd,  $J = 26.2, 6.6$  Hz, 8H).  $^{13}\text{C}$  NMR (126 MHz, DMSO- $d_6$ )  $\delta$ : 159.90, 148.87, 140.12, 113.61, 107.70, 48.02, 46.68.

#### 5.2.1.2.3 *N'*-Benzylidene-4-(pyridin-2-yl)piperazine-1-carbohydrazide (**12a**).

Brown solid, yield: 80%; Mp:  $185\text{--}187$  °C;  $R_{\text{f}} = 0.42$  (DCM:MeOH, 98:02 v/v); FT-IR (Alpha ATR,  $\nu$   $\text{cm}^{-1}$ ): 3210 (NH-str.), 2815 (C-H aromatic), 1680 (C=O.), 1590 (C=N),  $^1\text{H}$  NMR (500 MHz, DMSO- $d_6$ )  $\delta$ : 10.09 (s, 1H D<sub>2</sub>O exchangeable), 8.46–8.38 (m, 2H), 7.32 (d,  $J = 8.6$  Hz, 2H), 7.25–7.16 (m, 5H), 6.45 (s, 1H), 3.5 (d,  $J = 3.8$  Hz, 8H).  $^{13}\text{C}$  NMR (126 MHz, DMSO- $d_6$ )  $\delta$ : 159.64, 153.57, 148.02, 137.41, 133.97, 132.97, 127.87,

125.28, 116.41, 104.21, 44.97, 44.01. LC/MS (Q-TOF,  $m/z$ ): 310  $[M + H]^+$ . HPLC purity: 97.35%, retention time: 3.42 min.

**5.2.1.2.4 *N'*-(2,3-Dimethoxybenzylidene)-4-(pyridin-2-yl)piperazine-1-carbohydrazide (12b).**

Brown solid, yield: 74%; Mp: 182–184 °C;  $R_f$  = 0.52 (DCM:MeOH, 98:02 v/v); FT-IR (Alpha ATR,  $\nu$   $\text{cm}^{-1}$ ): 3212 (NH-str.), 2836 (C-H aromatic), 1665 (C=O.), 1575 (C=N);  $^1\text{H}$  NMR (500 MHz, DMSO- $d_6$ )  $\delta$ : 9.35 (s, 1H, D<sub>2</sub>O exchangeable), 8.24–8.16 (m, 2H), 7.92 (d,  $J$  = 7.6 Hz, 2H), 7.83–7.79 (m, 1H), 7.35 (s, 1H), 6.69 (s, 2H), 3.83 (d,  $J$  = 4.9 Hz, 8H), 3.53–3.49 (m, 6H);  $^{13}\text{C}$  NMR (126 MHz, DMSO- $d_6$ )  $\delta$ : 158.90, 157.21, 149.98, 148.87, 145.94, 140.12, 127.46, 122.28, 122.00, 114.38, 113.61, 107.70, 60.65, 56.79, 48.02, 46.68. LC/MS (Q-TOF,  $m/z$ ): 370  $[M + H]^+$ . HPLC purity: 99.53%, retention time: 3.32 min.

**5.2.1.2.5 *4*-(Pyridin-2-yl)-*N'*-(3,4,5-trimethoxybenzylidene)piperazine-1-carbohydrazide (12c).**

Brown solid, yield: 82%; Mp: 172–174 °C;  $R_f$  = 0.51 (DCM:MeOH, 98:02 v/v); FT-IR (Alpha ATR,  $\nu$   $\text{cm}^{-1}$ ): 3208 (NH-str.), 2857 (C-H aromatic), 1672 (C=O.), 1585 (C=N);  $^1\text{H}$  NMR (500 MHz, DMSO- $d_6$ )  $\delta$ : 9.95 (s, 1H, D<sub>2</sub>O exchangeable), 8.56–8.42 (m, 2H), 8.10–8.02 (m, 2H), 7.47 (d,  $J$  = 6.2 Hz, 2H), 7.27–7.21 (m, 1H), 4.36 (d,  $J$  = 4.2 Hz, 8H) 3.58 (s, 3H), 3.27 (s, 6H);  $^{13}\text{C}$  NMR (126 MHz, DMSO- $d_6$ )  $\delta$ : 161.70, 158.31, 151.21, 146.57, 138.22, 131.65, 112.41, 110.52, 60.65, 56.89, 48.02, 46.68, 44.13. LC/MS (Q-TOF,  $m/z$ ): 400  $[M + H]^+$ . HPLC purity: 99.95%, retention time: 3.21 min.

**5.2.1.2.6 *N'*-(4-Hydroxybenzylidene)-4-(pyridin-2-yl)piperazine-1-carbohydrazide (12d).**

White solid, yield: 81%; Mp: 188–190 °C;  $R_f$  = 0.51 (DCM:MeOH, 98:02 v/v); FT-IR (Alpha ATR,  $\nu$   $\text{cm}^{-1}$ ): 3440 (OH), 3220 (NH-str.), 2848 (C-H aromatic), 1695 (C=O.),



1580 (C=N);  $^1\text{H}$  NMR (500 MHz, DMSO- $d_6$ )  $\delta$ : 10.23 (s, 1H, D<sub>2</sub>O exchangeable), 8.30–8.22 (m, 2H), 8.03 (d,  $J = 6.6$  Hz, 2H), 7.87 (t,  $J = 8.7$  Hz, 2H), 7.36 (s, 1H), 6.93 (t,  $J = 7.6$  Hz, 2H), 4.56 (s, 1H), 3.80 (d,  $J = 3.4$  Hz, 8H);  $^{13}\text{C}$  NMR (126 MHz, DMSO- $d_6$ )  $\delta$ : 161.60, 157.42, 152.61, 135.47, 124.44, 120.22, 115.79, 113.61, 107.70, 44.32, 42.58. LC/MS (Q-TOF,  $m/z$ ): 326 [M + H]<sup>+</sup>. HPLC purity: 99.82%, retention time: 2.93 min.

**5.2.1.2.7 *N'*-(2-Hydroxybenzylidene)-4-(pyridin-2-yl)piperazine-1-carbohydrazide (12e).**

White solid, yield: 76%; Mp: 183–184 °C;  $R_f = 0.51$  (DCM:MeOH, 98:02 v/v); FT-IR (Alpha ATR,  $\nu$  cm<sup>-1</sup>): 3416 (OH), 3228 (NH-str.), 2854 (C-H aromatic), 1682 (C=O.), 1586 (C=N);  $^1\text{H}$  NMR (500 MHz, DMSO- $d_6$ )  $\delta$ : 10.10 (s, 1H, D<sub>2</sub>O exchangeable), 8.4–8.28 (m, 2H), 8.10 (d,  $J = 7.2$  Hz, 2H), 7.47–7.41 (m, 2H), 7.31 (s, 1H), 7.13–7.09 (m, 2H), 4.30 (s, 1H), 3.81 (d,  $J = 3.7$  Hz, 8H);  $^{13}\text{C}$  NMR (126 MHz, DMSO- $d_6$ )  $\delta$ : 160.40, 158.32, 157.21, 148.87, 146.84, 140.12, 129.75, 128.54, 121.19, 120.39, 117.38, 113.61, 47.62, 46.46. LC/MS (Q-TOF,  $m/z$ ): 326 [M + H]<sup>+</sup>. HPLC purity: 96.87%, retention time: 3.02 min.

**5.2.1.2.8 *N'*-(2,4-Dihydroxybenzylidene)-4-(pyridine-2-yl)piperazine-1-carbohydrazide (12f).**

White solid, yield: 73%; Mp: 185–187 °C;  $R_f = 0.50$  (DCM:MeOH, 98:02 v/v); FT-IR (Alpha ATR,  $\nu$  cm<sup>-1</sup>): 3462 (OH), 3240 (NH-str.), 2876 (C-H aromatic), 1665 (C=O.), 1578 (C=N);  $^1\text{H}$  NMR (500 MHz, DMSO- $d_6$ )  $\delta$ : 10.25 (s, 1H, D<sub>2</sub>O exchangeable), 8.80–8.82 (m, 2H), 8.10 (s, 1H), 7.92–7.86 (m, 2H), 7.47 (d,  $J = 6.5$  Hz, 2H), 6.78–6.69 (m, 1H), 4.34 (s, 2H), 3.80 (d,  $J = 4.6$  Hz, 8H);  $^{13}\text{C}$  NMR (126 MHz, DMSO- $d_6$ )  $\delta$ : 160.51, 158.90, 157.21, 148.87, 146.84, 140.12, 130.87, 113.19, 107.70, 103.04, 47.62, 46.68. LC/MS (Q-TOF,  $m/z$ ): 342 [M + H]<sup>+</sup>. HPLC purity: 99.81%, retention time: 2.89 min.

**5.2.1.2.9 *N'*-(3-Methylbenzylidene)-4-(pyridin-2-yl)piperazine-1-carbohydrazide (12g).**

White solid, yield: 79%; Mp: 181–183 °C;  $R_f$  = 0.59 (DCM:MeOH, 98:02 v/v); FT-IR (Alpha ATR,  $\nu$   $\text{cm}^{-1}$ ): 3215 (NH-str.), 2850 (C–H aromatic), 1692 (C=O.), 1599 (C=N);  $^1\text{H}$  NMR (500 MHz, DMSO- $d_6$ )  $\delta$ : 9.95 (s, 1H, D<sub>2</sub>O exchangeable), 8.40–8.32 (m, 2H), 7.55 (d,  $J$  = 11.7 Hz, 2H), 7.48–7.41 (m, 2H), 7.29 (s, 1H), 6.82 (s, 2H), 3.45 (d,  $J$  = 4.8 Hz, 8H), 3.10 (s, 3H);  $^{13}\text{C}$  NMR (126 MHz, DMSO- $d_6$ )  $\delta$ : 158.90, 157.21, 148.87, 144.61, 140.12, 137.80, 136.66, 129.71, 128.54, 123.54, 107.70, 48.02, 46.68, 21.21. LC/MS (Q-TOF,  $m/z$ ): 324 [M + H]<sup>+</sup>. HPLC purity: 97.13%, retention time: 3.86 min.

**5.2.1.2.10 *N'*-(4-Methylbenzylidene)-4-(pyridine-2-yl)piperazine-1-carbohydrazide (12h).**

White solid, yield: 82%; Mp: 189–191 °C;  $R_f$  = 0.59 (DCM:MeOH, 98:02 v/v); FT-IR (Alpha ATR,  $\nu$   $\text{cm}^{-1}$ ): 3208 (NH-str.), 2835 (C–H aromatic), 1690 (C=O.), 1595 (C=N);  $^1\text{H}$  NMR (500 MHz, DMSO- $d_6$ )  $\delta$ : 10.42 (s, 1H, D<sub>2</sub>O exchangeable), 8.26–8.06 (m, 2H), 7.58–7.44 (m, 3H), 7.23 (d,  $J$  = 7.9 Hz, 2H), 6.87 (d,  $J$  = 8.6 Hz, 1H), 6.67 (dd,  $J$  = 6.8, 5.1 Hz, 1H), 3.54 (d,  $J$  = 3.9 Hz, 8H), 2.32 (s, 3H);  $^{13}\text{C}$  NMR (126 MHz, DMSO- $d_6$ )  $\delta$ : 157.21, 148.87, 144.64, 140.12, 138.51, 131.90, 129.04, 127.55, 113.61, 106.68, 48.02, 46.46, 21.13. LC/MS (Q-TOF,  $m/z$ ): 324 [M + H]<sup>+</sup>. HPLC purity: 98.98%, retention time: 3.83 min.

**5.2.1.2.11 *N'*-(4-Nitrobenzylidene)-4-(pyridin-2-yl)piperazine-1-carbohydrazide (12i).**

Yellow solid, yield: 77%; Mp: 173–175 °C;  $R_f$  = 0.47 (DCM:MeOH, 98:02 v/v); FT-IR (Alpha ATR,  $\nu$   $\text{cm}^{-1}$ ): 3245 (NH-str.), 2890 (C–H aromatic), 1662 (C=O), 1602 (C=N);  $^1\text{H}$  NMR (500 MHz, DMSO- $d_6$ )  $\delta$ : 10.39 (s, 1H), 10.05 (s, 1H, D<sub>2</sub>O exchangeable), 7.38 (t,  $J$  = 8.9 Hz, 2H), 7.25 (s, 2H), 7.17 (t,  $J$  = 10.3 Hz, 2H), 6.96–6.89 (m, 2H), 3.84 (d,  $J$  = 4.1 Hz, 8H);  $^{13}\text{C}$  NMR (126 MHz, DMSO- $d_6$ )  $\delta$ : 161.90, 157.21, 148.87, 148.02,

144.64, 140.12, 139.94, 128.05, 124.59, 113.61, 107.70, 48.02, 46.68. LC/MS (Q-TOF,  $m/z$ ): 355  $[M + H]^+$ . HPLC purity: 99.05%, retention time: 2.86 min.

**5.2.1.2.12**      **4-(Pyridin-2-yl)-N'-(4-(trifluoromethyl)benzylidene)piperazine-1-carbohydrazide (12j).**

Brown solid, yield: 76%;  $R_f = 0.64$  (DCM:MeOH, 98:02 v/v); Mp: 183–185 °C; FT-IR (Alpha ATR,  $\nu$   $\text{cm}^{-1}$ ): 3265 (NH-str.), 2915 (C–H aromatic), 1652 (C=O.), 1585 (C=N);  $^1\text{H}$  NMR (500 MHz, DMSO- $d_6$ )  $\delta$ : 10.16 (s, 1H, D<sub>2</sub>O exchangeable), 8.50–8.44 (m, 2H), 8.14 (d,  $J = 10.84$  Hz, 2H), 7.60 (d,  $J = 5.4$  Hz, 2H), 7.47 (s, 1H), 7.38–7.23 (m, 2H), 3.80 (d,  $J = 3.1$  Hz, 8H);  $^{13}\text{C}$  NMR (126 MHz, DMSO- $d_6$ )  $\delta$ : 158.90, 157.21, 148.87, 144.64, 140.12, 135.97, 130.12 (q,  $J_{C-F} = 28.41$  Hz) 129.51, 127.37 (q,  $J_{C-F} = 4.50$  Hz), 119.04 (q,  $J_{C-F} = 272.30$  Hz), 48.02, 46.68 46.46. LC/MS (Q-TOF,  $m/z$ ): 378  $[M + H]^+$ . HPLC purity: 98.99%, retention time: 5.22 min.

**5.2.1.2.13**      **4-(Pyridin-2-yl)-N'-(4-(trifluoromethoxy)benzylidene)piperazine-1-carbohydrazide (12k).**

Brown solid, yield 69%; Mp: 189–191 °C;  $R_f = 0.69$  (DCM:MeOH, 98:02 v/v); FT-IR (Alpha ATR,  $\nu$   $\text{cm}^{-1}$ ): 3235 (NH-str.), 2945 (C–H aromatic), 1664 (C=O.), 1581 (C=N);  $^1\text{H}$  NMR (500 MHz, DMSO- $d_6$ )  $\delta$ : 10.60 (s, 1H, D<sub>2</sub>O exchangeable), 8.19 (s, 1H), 8.14 (dd,  $J = 4.7, 1.4$  Hz, 1H), 7.76 (d,  $J = 8.7$  Hz, 2H), 7.59–7.53 (m, 1H), 7.41 (d,  $J = 8.3$  Hz, 2H), 6.88 (d,  $J = 8.6$  Hz, 1H), 6.67 (dd,  $J = 6.9, 5.0$  Hz, 1H), 3.55 (s, 8H).  $^{13}\text{C}$  NMR (126 MHz, DMSO- $d_6$ )  $\delta$ : 159.30, 154.72, 149.04, 148.02, 141.41, 138.07, 134.80, 128.61, 121.77 (q,  $J_{C-F} = 215.39$  Hz), 121.53, 119.49, 113.73, 107.74, 44.92, 43.97. LC/MS (Q-TOF,  $m/z$ ): 394  $[M + H]^+$ . HPLC purity: 97.93%, retention time: 5.25 min.

**5.2.1.2.14** *N'*-(4-Chlorobenzylidene)-4-(pyridin-2-yl)piperazine-1-carbohydrazide (12l).

White solid, yield: 77%; Mp: 194–196 °C;  $R_f$  = 0.61 (DCM:MeOH, 98:02 v/v); FT-IR (Alpha ATR,  $\nu$   $\text{cm}^{-1}$ ): 3245 (NH-str.), 2916 (C–H aromatic), 1690 (C=O.), 1604 (C=N);  $^1\text{H}$  NMR (500 MHz, DMSO- $d_6$ )  $\delta$ : 10.01 (s, 1H, D<sub>2</sub>O exchangeable), 8.42 (s, 1H), 8.14 (t,  $J$  = 9.2 Hz, 2H), 7.49–7.36 (m, 2H), 7.19 (t,  $J$  = 6.4 Hz, 2H), 7.05 (d,  $J$  = 10.26 Hz, 2H), 3.76 (d,  $J$  = 3.4 Hz, 8H);  $^{13}\text{C}$  NMR (126 MHz, DMSO- $d_6$ )  $\delta$ : 159.16, 157.81, 156.21, 148.87, 144.64, 140.12, 135.13, 134.11, 129.60, 128.95, 113.61, 107.70, 48.02, 46.68. LC/MS (Q-TOF,  $m/z$ ): 344 [M + H]<sup>+</sup>. HPLC purity: 98.04%, retention time: 4.49 min.

**5.2.1.2.15** *N'*-(4-Fluorobenzylidene)-4-(pyridin-2-yl)piperazine-1-carbohydrazide (12m).

White solid, yield: 76%; Mp: 192–194 °C;  $R_f$  = 0.57 (DCM:MeOH, 98:02 v/v); FT-IR (Alpha ATR,  $\nu$   $\text{cm}^{-1}$ ): 3248 (NH-str.), 2940 (C–H aromatic), 1672 (C=O.), 1594 (C=N);  $^1\text{H}$  NMR (500 MHz, DMSO- $d_6$ )  $\delta$ : 10.01 (s, 1H, D<sub>2</sub>O exchangeable), 8.45 (d,  $J$  = 4.6 Hz, 2H), 8.20–8.12 (m, 1H), 7.77 (dd,  $J$  = 7.8, 1.2 Hz, 2H), 7.47 (dd,  $J$  = 7.5, 1.4 Hz, 2H), 7.37–7.24 (m, 2H), 3.80 (d,  $J$  = 3.6 Hz, 8H);  $^{13}\text{C}$  NMR (126 MHz, DMSO- $d_6$ )  $\delta$ : 158.90 (d,  $J_{\text{C-F}}$  = 230.62 Hz), 157.21, 148.87, 140.12, 134.57, 133.96, 132.15 (d,  $J_{\text{C-F}}$  = 2.2 Hz), 129.81, 128.52 (d,  $J_{\text{C-F}}$  = 7.2 Hz), 124.64, 113.61 (d,  $J_{\text{C-F}}$  = 32.1 Hz), 47.62, 46.46. LC/MS (Q-TOF,  $m/z$ ): 328 [M + H]<sup>+</sup>. HPLC purity: 99.07%, retention time: 3.65 min.

**5.2.1.2.16** *N'*-(4-Bromobenzylidene)-4-(pyridin-2-yl)piperazine-1-carbohydrazide (12n).

White solid, yield: 74%; Mp: 201–203 °C;  $R_f$  = 0.61 (DCM:MeOH, 98:02 v/v); FT-IR (Alpha ATR,  $\nu$   $\text{cm}^{-1}$ ): 3244 (NH-str.), 2966 (C–H aromatic), 1676 (C=O.), 1571 (C=N);

$^1\text{H}$  NMR (500 MHz, DMSO- $d_6$ )  $\delta$ : 10.57 (s, 1H, D<sub>2</sub>O exchangeable), 8.13 (d,  $J$  = 3.8 Hz, 2H), 7.65–7.52 (m, 5H), 6.87 (d,  $J$  = 8.6 Hz, 1H), 6.69–6.65 (m, 1H), 3.54 (s, 8H).  $^{13}\text{C}$  NMR (126 MHz, DMSO- $d_6$ )  $\delta$ : 159.30, 154.70, 148.03, 141.83, 138.08, 134.76, 132.17, 128.74, 122.64, 113.73, 107.74, 44.92, 43.97. LC/MS (Q-TOF,  $m/z$ ): 390 [M + 2]<sup>+</sup>. HPLC purity: 97.35%, retention time: 3.42 min.

**5.2.1.2.17 *N'*-(2,4-Difluorobenzylidene)-4-(pyridine-2-yl)piperazine-1-carbohydrazide (12o).**

White solid, yield: 75%; Mp: 204–206 °C;  $R_f$  = 0.58 (DCM:MeOH, 98:02 v/v); FT-IR (Alpha ATR,  $\nu$   $\text{cm}^{-1}$ ): 3250 (NH-str.), 2986 (C–H aromatic), 1684 (C=O.), 1590 (C=N);  $^1\text{H}$  NMR (500 MHz, DMSO- $d_6$ )  $\delta$ : 10.66 (s, 1H, D<sub>2</sub>O exchangeable), 8.34 (s, 1H), 8.13 (dd,  $J$  = 4.8, 1.2 Hz, 1H), 7.88 (dd,  $J$  = 15.5, 8.6 Hz, 1H), 7.59–7.52 (m, 1H), 7.37–7.30 (m, 1H), 7.17 (td,  $J$  = 8.6, 2.1 Hz, 1H), 6.87 (d,  $J$  = 8.6 Hz, 1H), 6.67 (dd,  $J$  = 6.8, 5.1 Hz, 1H), 3.55 (s, 8H).  $^{13}\text{C}$  NMR (126 MHz, DMSO- $d_6$ )  $\delta$ : 159.29 (dd,  $J_{C-F}$  = 224.3, 5.2 Hz), 154.53 (d,  $J_{C-F}$  = 7.4 Hz), 148.02 (dd,  $J_{C-F}$  = 230.96, 4.4 Hz), 138.07, 134.92 (t,  $J_{C-F}$  = 8.8 Hz), 113.74 (dd,  $J_{C-F}$  = 22.4, 3.6 Hz), 113.04, 112.84 (dd,  $J_{C-F}$  = 36.1, 7.2 Hz), 107.74, 104.78 (t,  $J_{C-F}$  = 18.8 Hz), 44.90, 43.92. LC/MS (Q-TOF,  $m/z$ ): 346 [M + H]<sup>+</sup>. HPLC purity: 99.92%, retention time: 3.37 min.

**5.2.1.2.18 2-Phenyl-5-(4-(pyridin-2-yl)piperazin-1-yl)-1,3,4-oxadiazole (13a).**

White solid, yield: 84%;  $R_f$  = 0.63 (EtOAc:hexane, 60:40 v/v); Mp: 236–238 °C; FT-IR (Alpha ATR,  $\nu$   $\text{cm}^{-1}$ ): 3130 (C–H aromatic), 1570 (C=N);  $^1\text{H}$  NMR (500 MHz, DMSO- $d_6$ )  $\delta$ : 8.12 (d,  $J$  = 5.4 Hz, 1H), 7.53–7.47 (m, 2H), 7.45–7.40 (t,  $J$  = 4.8 Hz, 1H), 7.38–7.33 (m, 2H), 7.31–7.27 (m, 1H), 6.76–6.68 (m, 1H), 6.66–6.61 (m, 1H), 3.74 (d,  $J$  = 24.6 Hz, 8H);  $^{13}\text{C}$  NMR (126 MHz, DMSO- $d_6$ )  $\delta$ : 164.87, 161.24, 159.18, 158.90, 148.86, 140.11, 131.58, 129.25, 127.06, 126.68, 113.61, 107.71, 48.46, 47.08. LC/MS (Q-TOF,  $m/z$ ): 308 [M + H]<sup>+</sup>. HPLC purity: 96.30%, retention time: 4.72 min.

**5.2.1.2.19**      **2-(2,3-Dimethoxyphenyl)-5-(4-(pyridine-2-yl)piperazine-1-yl)-1,3,4-oxadiazole (13b).**

White solid, yield: 81%; Mp 240–242 °C;  $R_f = 0.62$  (EtOAc:hexane, 60:40 v/v); FT-IR (Alpha ATR,  $\nu$   $\text{cm}^{-1}$ ): 1418 (C–H aromatic), 1435 (C=N);  $^1\text{H}$  NMR (500 MHz, DMSO- $d_6$ )  $\delta$ : 8.10 (d,  $J = 4.5$  Hz, 1H), 7.47 (d,  $J = 7.8$  Hz, 1H), 7.28–7.26 (m, 1H), 7.09–7.06 (t,  $J = 4.8$  Hz, 1H), 6.97–6.95 (m, 1H), 6.69–6.61 (m, 1H), 3.72 (d,  $J = 19.6$  Hz, 6H), 3.67–3.58 (m, 8H);  $^{13}\text{C}$  NMR (126 MHz, DMSO- $d_6$ )  $\delta$ : 161.95, 161.46, 158.90, 153.25, 150.40, 148.86, 144.58, 140.13, 123.97, 120.36, 120.08, 117.91, 113.61, 60.65, 56.77, 48.28, 47.80. LC/MS (Q-TOF,  $m/z$ ): 368  $[\text{M} + \text{H}]^+$ . HPLC purity: 96.52%, retention time: 4.65 min.

**5.2.1.2.20**      **2-(3,4,5-Trimethoxyphenyl)-5-(4-(pyridine-2-yl)piperazine-1-yl)-1,3,4-oxadiazole (13c).**

White solid, yield 84%; Mp: 208–210 °C;  $R_f = 0.59$  (EtOAc:hexane, 60:40 v/v); FT-IR (Alpha ATR,  $\nu$   $\text{cm}^{-1}$  3210 (C–H aromatic), 1526 (C=N);  $^1\text{H}$  NMR (500 MHz, DMSO- $d_6$ )  $\delta$ : 8.09 (d,  $J = 6.4$ , 1H), 7.48–7.45 (m, 1H), 6.97 (s, 2H), 6.70–6.67 (m, 1H), 6.62–6.60 (m, 1H), 3.81 (s, 9H), 3.73 (d,  $J = 18.2$  Hz, 8H);  $^{13}\text{C}$  NMR (126 MHz, DMSO- $d_6$ )  $\delta$ : 163.32, 161.24, 158.90, 158.04, 151.60, 148.88, 143.52, 140.11, 122.07, 113.64, 107.71, 107.07, 60.65, 56.46, 48.28, 47.85. LC/MS (Q-TOF,  $m/z$ ): 398  $[\text{M} + \text{H}]^+$ . HPLC purity: 97.76%, retention time: 3.84 min.

**5.2.1.2.21** **4-(5-(4-(Pyridin-2-yl)piperazin-1-yl)-1,3,4-oxadiazol-2-yl)phenol (13d).**

White solid, yield: 78%; Mp: 213–215 °C;  $R_f = 0.61$  (EtOAc:hexane, 60:40 v/v); FT-IR (Alpha ATR,  $\nu$   $\text{cm}^{-1}$ ): 3460 (OH), 3240 (C–H aromatic), 1545 (C=N);  $^1\text{H}$  NMR (500 MHz, DMSO- $d_6$ )  $\delta$ : 8.11 (d,  $J = 6.8$  Hz, 1H), 7.42 (d,  $J = 4.8$  Hz, 2H), 7.32–7.21 (m, 3H), 7.10–7.09 (m, 1H), 6.82–6.76 (m, 1H), 4.27 (s, 1H), 3.81 (d,  $J = 18.2$  Hz, 8H);  $^{13}\text{C}$  NMR (126 MHz, DMSO- $d_6$ )  $\delta$ : 163.16, 161.20, 161.07, 159.18, 158.89, 148.86, 140.11,

127.56, 117.40, 115.79, 113.63, 109.28, 107.71, 48.28, 47.82. LC/MS (Q-TOF,  $m/z$ ): 324 [M + H]<sup>+</sup>. HPLC purity: 99.90%, retention time: 4.2 min.

**5.2.1.2.22 2-(5-(4-(Pyridin-2-yl)piperazin-1-yl)-1,3,4-oxadiazol-2-yl)phenol (13e).**

White solid, yield: 72%; Mp: 202–204 °C;  $R_f$  = 0.61 (EtOAc:hexane, 60:40 v/v); FT-IR (Alpha ATR,  $\nu$  cm<sup>-1</sup>): 3510 (OH), 3224 (C–H aromatic), 1532 (C=N); <sup>1</sup>H NMR (500 MHz, DMSO-*d*<sub>6</sub>)  $\delta$ : 8.10 (d,  $J$  = 7.8, 1H), 7.46 (t,  $J$  = 6.8 Hz, 1H), 7.36 (d,  $J$  = 8.6 Hz, 2H), 6.89 (d,  $J$  = 6.8 Hz, 2H), 6.69–6.60 (m, 2H), 3.53 (d,  $J$  = 22.6 Hz, 8H), 3.49 (s, 1H); <sup>13</sup>C NMR (126 MHz, DMSO-*d*<sub>6</sub>)  $\delta$ : 163.35, 161.20, 158.90, 158.44, 148.88, 144.56, 140.13, 131.78, 130.14, 119.85, 118.82, 113.60, 111.68, 48.28, 47.82. LC/MS (Q-TOF,  $m/z$ ): 324 [M + H]<sup>+</sup>. HPLC purity: 96.10%, retention time: 4.0 min.

**5.2.1.2.23 4-(5-(4-(Pyridin-2-yl)piperazin-1-yl)-1,3,4-oxadiazol-2-yl)benzene-1,3-diol (13f).**

White solid, yield: 78%; Mp: 217–219 °C;  $R_f$  = 0.55 (EtOAc:hexane, 60:40 v/v); FT-IR (Alpha ATR,  $\nu$  cm<sup>-1</sup>): 3560 (OH), 3283 (C–H aromatic), 1560 (C=N); <sup>1</sup>H NMR (500 MHz, DMSO-*d*<sub>6</sub>)  $\delta$ : 8.25 (d,  $J$  = 7.9 Hz, 1H), 7.81 (s, 1H), 7.52 (s, 1H), 7.32 (d,  $J$  = 4.2 Hz, 1H), 7.21–7.16 (m, 1H), 7.09–6.92 (m, 1H), 6.85–6.72 (m, 1H), 4.27 (s, 2H), 3.84 (d,  $J$  = 23.8 Hz, 8H). <sup>13</sup>C NMR (126 MHz, DMSO-*d*<sub>6</sub>)  $\delta$ : 164.35, 161.24, 159.34, 158.90, 148.88, 144.49, 140.13, 129.79, 113.61, 109.12, 107.71, 105.15, 104.07, 49.09, 48.23. LC/MS (Q-TOF,  $m/z$ ): 340 [M + H]<sup>+</sup>. HPLC purity: 97.89%, retention time: 3.44 min.

**5.2.1.2.24 2-(4-(Pyridin-2-yl)piperazin-1-yl)-5-(*m*-tolyl)-1,3,4-oxadiazole (13g).**

White solid, yield: 82%; Mp: 204–206 °C;  $R_f$  = 0.67 (EtOAc:hexane, 60:40 v/v); FT-IR (Alpha ATR,  $\nu$  cm<sup>-1</sup>): 1454 (C–H aromatic), 1120 (C=N); <sup>1</sup>H NMR (500 MHz, DMSO-*d*<sub>6</sub>)  $\delta$ : 8.02 (d,  $J$  = 4.8 Hz, 1H), 7.85–7.76 (m, 2H), 7.60–7.52 (m, 2H), 7.32 (t,  $J$  = 8.6 Hz, 1H), 7.24 (d,  $J$  = 7.5 Hz, 1H), 7.16–7.09 (m, 1H), 3.82 (d,  $J$  = 22.8 Hz, 8H), 2.36 (s,

3H);  $^{13}\text{C}$  NMR (126 MHz,  $\text{DMSO-}d_6$ )  $\delta$ : 162.00, 161.20, 158.90, 157.48, 148.82, 140.15, 138.91, 131.06, 130.17, 127.89, 126.70, 126.58, 113.61, 107.71, 43.58, 42.48, 22.82. LC/MS (Q-TOF,  $m/z$ ): 322  $[\text{M} + \text{H}]^+$ . HPLC purity: 97.49%, retention time: 5.52 min.

#### 5.2.1.2.25 2-(4-(Pyridin-2-yl)piperazin-1-yl)-5-(*p*-tolyl)-1,3,4-oxadiazole (13h).

White solid, yield: 87%; Mp: 205–207 °C;  $R_f$  = 0.67 (EtOAc:hexane, 60:40 v/v); Yield 87%, TLC (EtOAc:hexane, 60:40 v/v)  $R_f$  = 0.69, Mp 205–207 °C; FT-IR (Alpha ATR,  $\nu$   $\text{cm}^{-1}$ ): 3228 (C–H aromatic), 1505 (C=N);  $^1\text{H}$  NMR (500 MHz,  $\text{DMSO-}d_6$ )  $\delta$ : 8.05 (d,  $J$  = 4.8 Hz, 1H), 7.86–7.81 (m, 3H), 7.22 (d,  $J$  = 7.2 Hz, 2H), 7.08 (d,  $J$  = 8.2 Hz, 1H), 6.67–6.64 (t,  $J$  = 4.2 Hz, 1H), 3.59 (d,  $J$  = 24.6 Hz, 8H), 2.30 (s, 3H);  $^{13}\text{C}$  NMR (126 MHz,  $\text{DMSO-}d_6$ )  $\delta$ : 162.18, 160.97, 159.14, 158.53, 148.90, 140.64, 139.13, 129.45, 126.91, 124.97, 113.63, 107.09, 47.20, 46.04, 22.82. LC/MS (Q-TOF,  $m/z$ ): 322  $[\text{M} + \text{H}]^+$ . HPLC purity: 98.16%, retention time: 5.61 min.

#### 5.2.1.2.26 2-(4-Nitrophenyl)-5-(4-(pyridin-2-yl)piperazin-1-yl)-1,3,4-oxadiazole (13i).

White solid, yield: 75%;  $R_f$  = 0.71 (EtOAc:hexane, 60:40 v/v); Mp: 213–215 °C; FT-IR (Alpha ATR,  $\nu$   $\text{cm}^{-1}$ ): 3269 (C–H aromatic), 1564 (C=N);  $^1\text{H}$  NMR (500 MHz,  $\text{DMSO-}d_6$ )  $\delta$ : 8.28 (d,  $J$  = 7.5 Hz, 2H), 8.18 (d,  $J$  = 8.9 Hz, 1H), 7.83 (d,  $J$  = 8.9 Hz, 2H), 7.67 (t,  $J$  = 4.5 Hz, 1H), 7.48–7.45 (t,  $J$  = 4.8 Hz, 1H), 6.49–6.43 (m, 1H), 3.96 (d,  $J$  = 22.8 Hz, 8H);  $^{13}\text{C}$  NMR (126 MHz,  $\text{DMSO-}d_6$ )  $\delta$ : 165.46, 162.00, 159.91, 158.86, 149.35, 147.05, 140.19, 132.79, 127.12, 124.66, 113.03, 107.43, 48.39, 46.81. LC/MS (Q-TOF,  $m/z$ ): 353  $[\text{M} + \text{H}]^+$ . HPLC purity: 99.90%, retention time: 4.05 min.

#### 5.2.1.2.27 2-(4-(Pyridin-2-yl)piperazin-1-yl)-5-(4-(trifluoromethyl)phenyl)-1,3,4-oxadiazole (13j).

White solid, yield: 73%; Mp: 221–223 °C;  $R_f$  = 0.73 (EtOAc:hexane, 60:40 v/v); FT-IR (Alpha ATR,  $\nu$   $\text{cm}^{-1}$ ): 3176 (C–H aromatic), 1538 (C=N);  $^1\text{H}$  NMR (500 MHz,  $\text{DMSO-}$



$d_6$ )  $\delta$ : 8.12 (d,  $J = 8.4$  Hz, 1H), 7.69 (d,  $J = 7.1$  Hz, 2H), 7.48–7.42 (m, 1H), 7.12–7.04 (m, 1H), 6.78 (t,  $J = 7.1$  Hz, 2H), 6.34–6.24 (m, 1H), 3.67 (d,  $J = 24.6$ , 8H);  $^{13}\text{C}$  NMR (126 MHz, DMSO- $d_6$ )  $\delta$ : 164.37, 162.53, 159.88, 154.83, 137.45 (q,  $J_{\text{C-F}} = 3.2$  Hz), 128.92 (q,  $J_{\text{C-F}} = 28.8$  Hz), 126.33 (q,  $J_{\text{C-F}} = 8.6$  Hz), 124.66, 124.32, 113.08, 107.41, 48.39, 46.81. LC/MS (Q-TOF,  $m/z$ ): 376  $[\text{M} + \text{H}]^+$ . HPLC purity: 95.17%, retention time: 6.26 min.

**5.2.1.2.28**     *2-(4-(Pyridin-2-yl)piperazin-1-yl)-5-(4-(trifluoromethoxy)phenyl)-1,3,4-oxadiazole (13k).*

White solid, yield 72%; Mp: 216–218 °C;  $R_f = 0.66$  (EtOAc:hexane, 60:40 v/v); FT-IR (Alpha ATR,  $\nu \text{ cm}^{-1}$ ): 3281 (C–H aromatic), 1550 (C=N);  $^1\text{H}$  NMR (500 MHz, DMSO- $d_6$ )  $\delta$ : 8.15 (dd,  $J = 4.9, 1.3$  Hz, 1H), 8.06–8.01 (m, 2H), 7.61–7.52 (m, 3H), 6.92 (d,  $J = 8.6$  Hz, 1H), 6.70 (dd,  $J = 6.8, 5.1$  Hz, 1H), 3.65 (dd,  $J = 7.1, 4.0$  Hz, 8H);  $^{13}\text{C}$  NMR (126 MHz, DMSO- $d_6$ )  $\delta$ : 164.55, 159.12, 157.98, 148.06, 138.23, 128.06 (q,  $J_{\text{C-F}} = 254.6$  Hz), 123.73, 122.23, 114.01, 107.96, 45.81, 44.20. LC/MS (Q-TOF,  $m/z$ ): 392  $[\text{M} + \text{H}]^+$ . HPLC purity: 99.90%, retention time: 5.66 min.

**5.2.1.2.29**     *2-(4-Chlorophenyl)-5-(4-(pyridin-2-yl)piperazin-1-yl)-1,3,4-oxadiazole (13l).*

White solid, yield: 73%; Mp: 201–203 °C;  $R_f = 0.68$  (EtOAc:hexane, 60:40 v/v); FT-IR (Alpha ATR,  $\nu \text{ cm}^{-1}$ ): 3392 (C–H aromatic), 1580 (C=N);  $^1\text{H}$  NMR (500 MHz, DMSO- $d_6$ )  $\delta$  8.09 (d,  $J = 7.5$  Hz, 1H), 7.48–7.41 (m, 5H), 6.69–6.68 (m, 1H), 6.62–6.60 (m, 1H), 3.84 (d,  $J = 18.8$  Hz, 8H);  $^{13}\text{C}$  NMR (126 MHz, DMSO- $d_6$ )  $\delta$ : 164.13, 161.15, 159.32, 158.98, 148.98, 140.11, 137.38, 129.49, 124.40, 112.48, 103.21, 49.12, 47.71. LC/MS (Q-TOF,  $m/z$ ): 342  $[\text{M} + \text{H}]^+$ . HPLC purity: 98.02%, retention time: 4.59 min.

**5.2.1.2.30**      **2-(4-Fluorophenyl)-5-(4-(pyridin-2-yl)piperazin-1-yl)-1,3,4-oxadiazole (13m).**

White solid, yield: 78%; Mp: 194–196 °C;  $R_f$  = 0.65 (EtOAc:hexane, 60:40 v/v); FT-IR (Alpha ATR,  $\nu$   $\text{cm}^{-1}$ ): 3315 (C–H aromatic), 1635 (C=N);  $^1\text{H}$  NMR (500 MHz, DMSO- $d_6$ )  $\delta$ : 8.11 (d,  $J$  = 5.5 Hz, 1H), 7.56 (t,  $J$  = 8.9 Hz, 2H), 7.38 (t,  $J$  = 6.8 Hz, 2H), 7.10–7.01 (m, 1H), 6.54–6.48 (m, 1H), 6.31–6.24 (m, 1H), 3.95 (d,  $J$  = 34.1, 4.6 Hz, 8H);  $^{13}\text{C}$  NMR (126 MHz, DMSO- $d_6$ )  $\delta$ : 164.03, 163.08 (d,  $J_{\text{C-F}}$  = 230.5 Hz), 156.44, 140.33, 132.70 (d,  $J_{\text{C-F}}$  = 3.6 Hz), 132.30, 128.22 (d,  $J_{\text{C-F}}$  = 2.6 Hz), 128.08, 126.01, 114.98 (d,  $J_{\text{C-F}}$  = 18.3 Hz), 48.94, 47.55. LC/MS (Q-TOF,  $m/z$ ): 326  $[\text{M} + \text{H}]^+$ . HPLC purity 98.84%, retention time: 5.25 min.

**5.2.1.2.31**      **2-(4-Bromophenyl)-5-(4-(pyridin-2-yl)piperazin-1-yl)-1,3,4-oxadiazole (13n).**

White solid, yield: 76%; Mp: 189–191 °C;  $R_f$  = 0.71 (EtOAc:hexane, 60:40 v/v); FT-IR (Alpha ATR,  $\nu$   $\text{cm}^{-1}$ ): 3345 (C–H aromatic), 1628 (C=N);  $^1\text{H}$  NMR (500 MHz,  $\text{CDCl}_3$ )  $\delta$  8.24 (dd,  $J$  = 5.2, 1.5 Hz, 1H), 7.86–7.79 (m, 2H), 7.65–7.60 (m, 2H), 7.56 (dd,  $J$  = 8.8, 7.2 Hz, 1H), 6.74 (d,  $J$  = 8.6 Hz, 2H), 3.74 (s, 8H);  $^{13}\text{C}$  NMR (126 MHz,  $\text{CDCl}_3$ )  $\delta$ : 164.18, 159.01, 158.82, 152.07, 148.08, 137.80, 132.19, 127.25, 125.01, 123.41, 114.23, 107.46, 45.90, 44.57. LC/MS (Q-TOF,  $m/z$ ): 388  $[\text{M} + 2]^+$ . HPLC purity: 97.49%, retention time: 5.52 min.

**5.2.1.2.32**      **2-(2,4-Difluorophenyl)-5-(4-(pyridin-2-yl)piperazin-1-yl)-1,3,4-oxadiazole (13o).**

White solid, yield: 73%; Mp: 181–183 °C;  $R_f$  = 0.66 (EtOAc:hexane, 60:40 v/v); FT-IR (Alpha ATR,  $\nu$   $\text{cm}^{-1}$ ): 3367 (C–H aromatic), 1643 (C=N);  $^1\text{H}$  NMR (500 MHz, DMSO- $d_6$ )  $\delta$ : 8.14–8.12 (m, 1H), 8.05–7.96 (m, 1H), 7.61–7.48 (m, 2H), 7.30 (td,  $J$  = 8.3, 2.3 Hz, 1H), 6.91 (d,  $J$  = 8.6 Hz, 1H), 6.69 (dd,  $J$  = 6.9, 5.0 Hz, 1H), 3.63 (dd,  $J$  = 7.2, 4.4

Hz, 8H).  $^{13}\text{C}$  NMR (126 MHz, DMSO- $d_6$ )  $\delta$ : 159.10 (dd,  $J_{C-F}$  = 240.6, 7.2 Hz), 154.66, 146.05 (d,  $J_{C-F}$  = 7.4 Hz), 138.22, 130.85 (t,  $J_{C-F}$  = 8.4 Hz), 130.76, 114.01 (dd,  $J_{C-F}$  = 34.2, 7.2 Hz), 113.30, 113.13, 107.95 (t,  $J_{C-F}$  = 18.3 Hz), 106.05, 105.84, 45.83, 44.19. LC/MS (Q-TOF,  $m/z$ ): 344  $[\text{M} + \text{H}]^+$ . HPLC purity: 97.13%, retention time: 3.86 min.

## 5.2.2 Biological evaluation

### 5.2.2.1 In-vitro biological evaluation

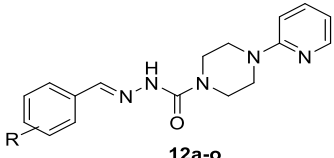
#### 5.2.2.1.1 Cholinesterase (hAChE and hBChE) and hBACE-1 inhibition activities

Multifunctional activities of synthesized compounds **12a-o** and **13a-o** were evaluated against human cholinesterase (hAChE, hBChE), and hBACE-1. The results are summarized in Table 5.4. The tested compounds exhibited poor to excellent inhibition against hAChE with  $\text{IC}_{50}$  values ranging from two digits nanomolar range to  $> 10 \mu\text{M}$ . The compounds **12a-o** showed hAChE inhibition in micromolar level except compounds **12n** ( $\text{IC}_{50} = 0.489 \mu\text{M}$ ) and **12o** ( $\text{IC}_{50} = 0.682 \mu\text{M}$ ) owing to the substitution of electron-withdrawing groups (EWGs), 4-Br and 2,4-diF, respectively. Unsurprisingly, the replacement of imine linker with oxadiazole ring (compounds **13a-o**) increased inhibitory potential to several folds. In the compounds having the presence of oxadiazole ring, the unsubstituted compound (**13a**) displayed moderate hAChE inhibition with an  $\text{IC}_{50}$  value of  $0.341 \mu\text{M}$ . Further, the substitution of EDGs resulted in a drastic decline in hAChE inhibition except 3,4,5-triOMe substituted compound (**13c**), which showed a slightly higher inhibition ( $\text{IC}_{50} = 0.222 \mu\text{M}$ ). The substitution of the terminal phenyl group with EWGs exponentially increased the anti-hAChE activity. The compounds with substitution of 4- $\text{NO}_2$  (**13i**,  $\text{IC}_{50} = 0.219 \mu\text{M}$ ), 4- $\text{CF}_3$  (**13j**,  $\text{IC}_{50} = 0.182 \mu\text{M}$ ), 4-Cl (**13l**,  $\text{IC}_{50} = 0.102 \mu\text{M}$ ), and 4-Br (**13m**,  $\text{IC}_{50} = 0.136 \mu\text{M}$ ) functionalities presented very good anti-hAChE activity in three-digit nanomolar range. Moreover, **13k** ( $\text{IC}_{50} = 0.089 \mu\text{M}$ ), **13n** ( $\text{IC}_{50} = 0.074 \mu\text{M}$ ), and **13o** ( $\text{IC}_{50} = 0.054 \mu\text{M}$ ) were the best

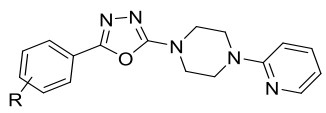
compounds of the series having presence of 4-OCF<sub>3</sub>, 4-Br, and 2,4-diF, respectively with excellent hAChE inhibition in two-digit nanomolar range. All the tested compounds exhibited comparatively lower hBChE inhibition than hAChE except compound **12c**, which has more selectivity toward hBChE. All compounds exhibited hBChE inhibition in micromolar levels except compounds **13n** (IC<sub>50</sub> = 0.846 μM), and **13o** (IC<sub>50</sub> = 0.787 μM).

In addition to hAChE and hBChE, hBACE-1 inhibitory potential of compounds was evaluated. BACE-1 is responsible for catalytic proteolysis of APP into insoluble fragments of Aβ. Similar to hAChE activity, imines (**12a-o**) exhibited lower hBACE-1 inhibition compared to their oxadiazole congeners (**13a-o**). Only the exception being compound **12k** (IC<sub>50</sub> = 0.248 μM) having 4-OCF<sub>3</sub> substitution at phenyl ring showed slightly higher activity than oxadiazole counterpart (**13k**: IC<sub>50</sub> = 0.822 μM). The unsubstituted compounds **12a** (IC<sub>50</sub> = 7.69 μM), and **13a** (IC<sub>50</sub> = 3.22 μM) showed lower anti-hBACE-1 activity than substituted analogs. Most of the compounds (**13a**, **13c**, **13i**, **13l**, and **13m**) exhibited very good hAChE inhibition with IC<sub>50</sub> in three digit nanomolar concentration, but unfortunately, very low potential against hBACE-1 (IC<sub>50</sub> > 1 μM). Conversely, two of the compounds **12k** (IC<sub>50</sub> = 0.486 μM) and **13f** (IC<sub>50</sub> = 0.382 μM) displayed excellent hBACE-1 inhibition, but remarkably decreased anti-hAChE activity (IC<sub>50</sub> > 1 μM). Apart from compounds **12k**, and **13f**, six more compounds **12n** (IC<sub>50</sub> = 0.296 μM), **12o** (IC<sub>50</sub> = 0.446 μM), **13j** (IC<sub>50</sub> = 0.465 μM), **13k** (IC<sub>50</sub> = 0.822 μM), **13n** (IC<sub>50</sub> = 0.126 μM), and **13o** (IC<sub>50</sub> = 0.098 μM) displayed significant hBACE-1 inhibition with IC<sub>50</sub> in three-digit nanomolar range. The common compounds (**12n**, **12o**, **13j**, **13k**, **13n**, and **13o**) were selected as multifunctional lead candidates by the virtue of balanced and significant inhibition of hAChE, hBChE and hBACE-1 to be investigated further.

**Table 5.4.** Cholinesterases (hAChE and hBChE) and hBACE-1 inhibition activity and selectivity index of compounds (Series III and IV).



**12a-o**



**13a-o**

Comd.	R-Group	IC <sub>50</sub> ± SEM (μM) <sup>a</sup>			hAChE SI <sup>b</sup>	LogP <sup>d</sup>
		hAChE	hBChE	hBACE-1		
<b>12a</b>	H	3.62 ± 0.089	4.22 ± 0.068	7.69 ± 0.206	1.2	2.82
<b>12b</b>	2,3-diOMe	>10	>10	6.82 ± 0.283	--	2.57
<b>12c</b>	3,4,5-triOMe	5.69 ± 0.092	4.68 ± 0.048	4.64 ± 0.118	0.8	2.44
<b>12d</b>	4-OH	4.81 ± 0.086	6.15 ± 0.034	4.68 ± 0.162	1.3	2.43
<b>12e</b>	2-OH	>10	>10	5.88 ± 0.196	--	2.48
<b>12f</b>	2,4-diOH	4.68 ± 0.049	4.82 ± 0.066	4.64 ± 0.182	1.0	2.04
<b>12g</b>	3-Me	>10	> 10	4.37 ± 0.115	--	3.31
<b>12h</b>	4-Me	4.78 ± 0.064	> 10	3.92 ± 0.119	--	3.36
<b>12i</b>	4-NO <sub>2</sub>	1.16 ± 0.008	4.02 ± 0.082	2.64 ± 0.127	3.5	1.61
<b>12j</b>	4-CF <sub>3</sub>	1.32 ± 0.009	4.04 ± 0.096	1.82 ± 0.090	3.1	3.74
<b>12k</b>	4-OCF <sub>3</sub>	2.91 ± 0.036	4.35 ± 0.102	0.248 ± 0.006	1.5	4.35
<b>12l</b>	4-Cl	3.42 ± 0.042	4.82 ± 0.081	2.96 ± 0.136	1.4	3.38
<b>12m</b>	4-F	1.87 ± 0.018	3.99 ± 0.161	1.24 ± 0.046	2.1	2.98
<b>12n</b>	4-Br	0.489 ± 0.008	1.88 ± 0.064	0.296 ± 0.009	3.8	3.35
<b>12o</b>	2,4-diF	0.682 ± 0.003	3.97 ± 0.092	0.446 ± 0.021	5.8	3.14
<b>13a</b>	H	0.341 ± 0.004	3.27 ± 0.081	3.22 ± 0.089	9.6	3.69
<b>13b</b>	2,3-diOMe	1.19 ± 0.003	5.22 ± 0.186	2.16 ± 0.092	4.4	3.44
<b>13c</b>	3,4,5-triOMe	0.222 ± 0.004	3.64 ± 0.069	3.24 ± 0.132	16.4	3.31
<b>13d</b>	4-OH	1.18 ± 0.012	6.02 ± 0.102	1.78 ± 0.086	5.1	3.33
<b>13e</b>	2-OH	1.23 ± 0.009	8.22 ± 0.361	2.23 ± 0.112	6.7	3.36
<b>13f</b>	2,4-diOH	1.34 ± 0.006	3.29 ± 0.142	0.382 ± 0.015	2.5	2.91
<b>13g</b>	3-Me	5.24 ± 0.009	> 10	2.64 ± 0.108	--	4.18
<b>13h</b>	4-Me	1.02 ± 0.009	>10	2.48 ± 0.104	--	4.20
<b>13i</b>	4-NO <sub>2</sub>	0.219 ± 0.006	2.86 ± 0.068	1.34 ± 0.064	13.1	3.62
<b>13j</b>	4-CF <sub>3</sub>	0.182 ± 0.005	2.12 ± 0.091	0.465 ± 0.022	11.6	4.61
<b>13k</b>	4-OCF <sub>3</sub>	0.089 ± 0.003	1.96 ± 0.082	0.822 ± 0.026	22.0	5.22
<b>13l</b>	4-Cl	0.102 ± 0.002	1.82 ± 0.072	1.32 ± 0.028	17.8	4.25
<b>13m</b>	4-F	0.136 ± 0.005	1.22 ± 0.049	1.48 ± 0.064	9.0	3.85
<b>13n</b>	4-Br	0.074 ± 0.004	0.846 ± 0.037	0.126 ± 0.009	11.4	4.52
<b>13o</b>	2,4-diF	0.054 ± 0.002	0.787 ± 0.022	0.098 ± 0.004	14.6	4.01
	Donepezil <sup>c</sup>	0.042 ± 0.002	2.42 ± 0.082	0.362 ± 0.017	57.6	
	Rivastigmine <sup>c</sup>	1.68 ± 0.008	1.22 ± 0.061	--	0.7	

<sup>a</sup>Data are represented as the mean IC<sub>50</sub> ± SEM of three separate experiments (n = 3); <sup>b</sup>selectivity ratio = IC<sub>50</sub> of hBChE/hAChE; <sup>c</sup>Ref. [Sharma et al. 2019b] nd = not determined. <sup>d</sup>Log P value was determined using the shake flask method.

### 5.2.2.1.2 Enzyme kinetics study

The enzyme kinetics study was performed to evaluate the mechanism of type of inhibition for most potential compound **13o** against hAChE. The Lineweaver-Burk plot was constructed for three varying concentrations of test compounds against six different concentrations of substrate (acetylthiocholine iodide, ATCI). The results showed decreased  $V_{\max}$ , whereas  $K_m$  values increased with increasing concentration of inhibitor (Figure 5.13). The Dixon plot showed that compound **13o** has  $K_i = 0.030 \mu\text{M}$  (Figure 5.14).

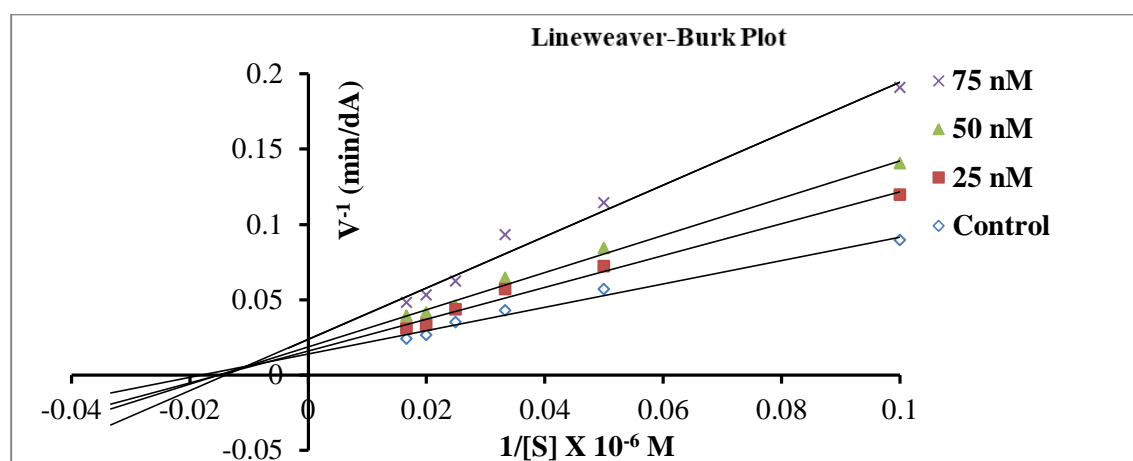


**Figure 5.13.** Enzyme kinetics study of compound **13o** against hAChE showing mixed-type of inhibition Lineweaver-Burk plot.

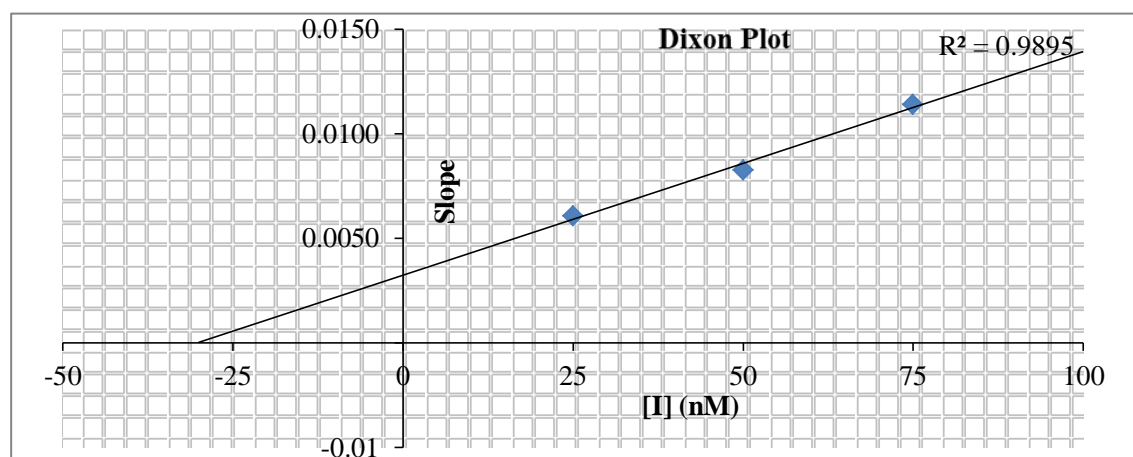


**Figure 5.14.** Dixon plot determined the dissociation constant  $K_i$  of compound **13o** at three different concentrations (0.025, 0.050, and 0.075  $\mu\text{M}$ ).

### 5.2.2.1.3 Propidium iodide displacement assay

The PAS-hAChE binding capability of compounds (**12n**, **12o**, **13j**, **13k**, **13n**, and **13o**) was evaluated by propidium iodide displacement assay at the concentrations of 10 and 50  $\mu\text{M}$ . Propidium iodide is known ligand that specifically binds to PAS region of hAChE. The results of assay indicated lower displacement of propidium iodide from compounds **12n**, **12o**, **13j**, and **13k** compared to donepezil, while compound **13n** (10  $\mu\text{M}$  = 18.1%; 50  $\mu\text{M}$  = 31.4%) showed comparable activity. Interestingly, compound **13o** (10  $\mu\text{M}$  = 22.4%; 50  $\mu\text{M}$  = 36.6%) displayed higher propidium iodide displacement activity than donepezil (10  $\mu\text{M}$  = 16.9%; 50  $\mu\text{M}$  = 32.0%)

Overall results suggested that compounds **13n** and **13o** exhibited balanced and significant inhibition of hAChE and hBACE-1 along with the capability to displace propidium iodide from PAS-AChE with excellent brain permeability characteristics. Thereby, compounds **13n** and **13o** selected as most potential leads for further pharmacological investigations.

### 5.2.2.1.4 Parallel artificial membrane permeation assay (PAMPA-BBB)

The brain permeability of compounds is the essential prerequisites of CNS acting drugs. Parallel artificial membrane permeation assay (PAMPA) was performed to assess the blood-brain barriers (BBB) permeability of selected potential compounds by the reported method of Di et al. [Di et al. 2003]. The assay protocol was validated by comparing the experimental results ( $P_{e(\text{exp})}$ ) with reported results ( $P_{e(\text{ref})}$ ) of the permeability of nine commercial drugs. A linear correlation  $P_{e(\text{exp})} = 1.308P_{e(\text{ref})} - 0.8394$ , ( $R^2 = 0.9317$ ) was established, which suggested permeability limit of  $P_e > 4.3 \times 10^{-6} \text{ cm.s}^{-1}$  for appreciable CNS permeability, while value between  $P_e < 4.3 - 1.3 \times 10^{-6} \text{ cm.s}^{-1}$  for uncertain CNS permeability. The results of the assay indicated excellent brain permeability by compounds **13j**, **13k**, **13n**, and **13o**, while compounds **12n** and **12o**

showed uncertain permeability (Table 5.5). The higher permeability of compounds **13j**, **13k**, **13n**, and **13o** also signified the benefits of cyclization of carboxamide imine into oxadiazole.

**Table 5.5.** Propidium iodide displacement and predicted BBB permeability (Series III-IV).

Comd.	Propidium iodide displacement from AChE PAS (% inhibition) <sup>a</sup>		PAMPA-BBB permeability	
	At 10 $\mu$ M	At 50 $\mu$ M	$P_{e(exp)}$ ( $10^{-6}$ cm.s <sup>-1</sup> )	Permeability prediction
<b>12n</b>	10.4 $\pm$ 0.4	13.9 $\pm$ 0.46	3.6 $\pm$ 0.16	CNS $\pm^c$
<b>12o</b>	12.7 $\pm$ 0.3	22.6 $\pm$ 0.87	4.1 $\pm$ 0.12	CNS $\pm^c$
<b>13j</b>	14.2 $\pm$ 0.4	19.8 $\pm$ 0.71	6.3 $\pm$ 0.19	CNS+ <sup>b</sup>
<b>13k</b>	16.8 $\pm$ 0.6	23.9 $\pm$ 0.92	6.8 $\pm$ 0.12	CNS+ <sup>b</sup>
<b>13n</b>	18.1 $\pm$ 0.4	31.4 $\pm$ 0.67	5.9 $\pm$ 0.08	CNS+ <sup>b</sup>
<b>13o</b>	22.4 $\pm$ 0.3	36.6 $\pm$ 0.81	6.1 $\pm$ 0.17	CNS+ <sup>b</sup>
donepezil	16.9 $\pm$ 0.2	32.0 $\pm$ 0.77	7.6 $\pm$ 0.16	CNS+ <sup>b</sup>

<sup>a</sup>The propidium iodide displacement assay was performed at 10  $\mu$ M and 50  $\mu$ M concentrations of respective inhibitors. <sup>b</sup>‘CNS+’ suggested excellent ( $P_e > 4.4 \times 10^{-6}$  cm s<sup>-1</sup>) and <sup>c</sup>‘CNS $\pm$ ’ suggested uncertain ( $4.4$  to  $1.8 \times 10^{-6}$  cm s<sup>-1</sup>) brain permeability values. Data are expressed as the mean  $\pm$  SEM of three separate experiments ( $n = 3$ ).

#### 5.2.2.1.5 Self-and AChE-induced A $\beta$ aggregation inhibition by thioflavin T assay

The deposition and aggregation of A $\beta$  can be considered as a major detrimental factor in AD [Sadigh-Eteghad et al. 2015]. The results of hAChE and hBACE-1 inhibitory potential and PAS-hAChE binding capability have prompted us to evaluate the anti-A $\beta$  aggregation activity of compounds **13n** and **13o**. The thioflavin T assay was performed to determine the self- and AChE-induced A $\beta$  aggregation inhibition activity at the concentration ratios of A $\beta$  and inhibitor (10:5  $\mu$ M, 10:10  $\mu$ M, and 10:20  $\mu$ M, respectively) and the results were reported as percentage anti-A $\beta$  aggregation (Figures 5.15A and 5.15B) and normalized fluorescence intensity (NFI) (Figures 5.16A and 5.16B). The results demonstrated concentration-dependent inhibition of A $\beta$  aggregation with the maximum activity was observed at 20  $\mu$ M inhibitor (A $\beta$ : inhibitor, 10:20  $\mu$ M). The results revealed remarkably higher A $\beta$  inhibition by compound **13o** with NFI values of 0.62–0.30 and 0.63–0.34 in self- and AChE- induced experiments, respectively and



was comparable with donepezil (self-induced: 0.59–0.31 hAChE-induced: 0.78–0.48), while compound **13n** showed slightly lower inhibition in self- (0.66–0.42) and hAChE-induced (0.84–0.60) experiments compared to donepezil. The results were also observed in accordance with *in-vitro* hAChE and BACE-1 assays and signified PAS-hAChE binding might be a responsible factor in inhibiting A $\beta$  aggregation.

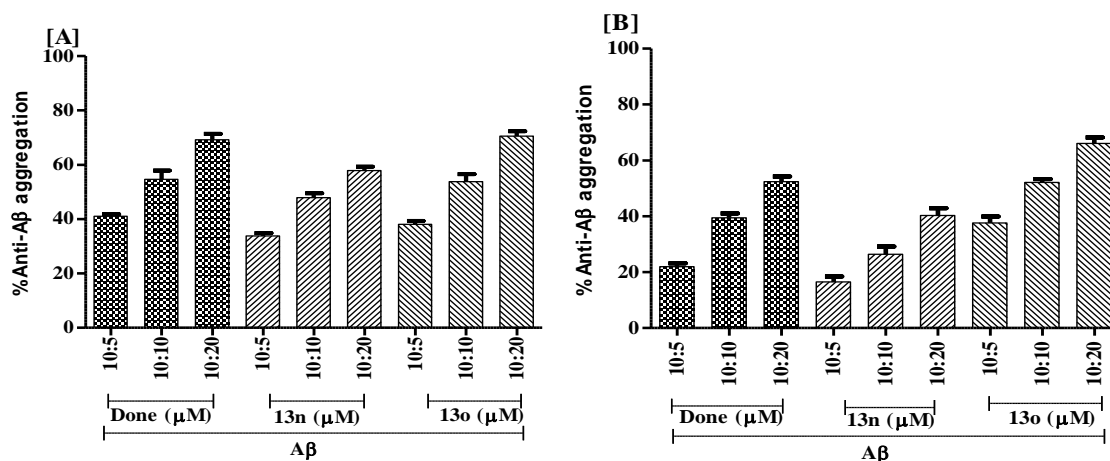


**Figure 5.15.** The results of % anti-A $\beta$  aggregation activity in thioflavin T assay. Data are expressed as the mean  $\pm$  SEM of three separate experiments ( $n = 3$ ).

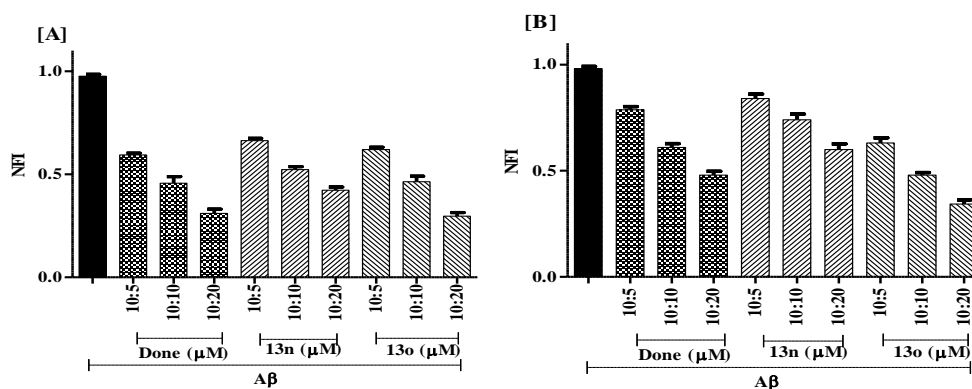


**Figure 5.16.** Results of thioflavin T assay for compounds **13n** and **13o** in [A] self-induced; [B] AChE-induced experiments. Each bar displays the values of normalized fluorescence intensity (NFI) as the mean  $\pm$  SEM of three separate experiments ( $n = 3$ ).

#### 5.2.2.1.6 AFM study

The morphological characterization of A $\beta$  aggregates in the presence or absence of inhibitor was performed by atomic force microscopy (AFM) to examine the impact of A $\beta$  aggregation inhibition at different time points (0, 4, and 7 days). Detailed structural

analysis of A $\beta$  aggregates like the formation of fibrils and large oligomers was visually confirmed by AFM images and expressed in terms of maximum peak height and roughness index. The value of peak heights and roughness index were considered to be directly proportional to the aggregation of A $\beta$ . The results reflected that the peak heights (23.32–423.6 nm) and roughness index (1.56–41.12 nm) of A $\beta$  without inhibitor was drastically higher than the presence of inhibitor (maximum peak height: 44.23–162.97 nm; roughness index: 1.84–4.69 nm). The reduction in maximum peak height and roughness index due to the presence of an inhibitor ascertained the anti-A $\beta$  aggregatory activity by **13o** (Figure 5.17).

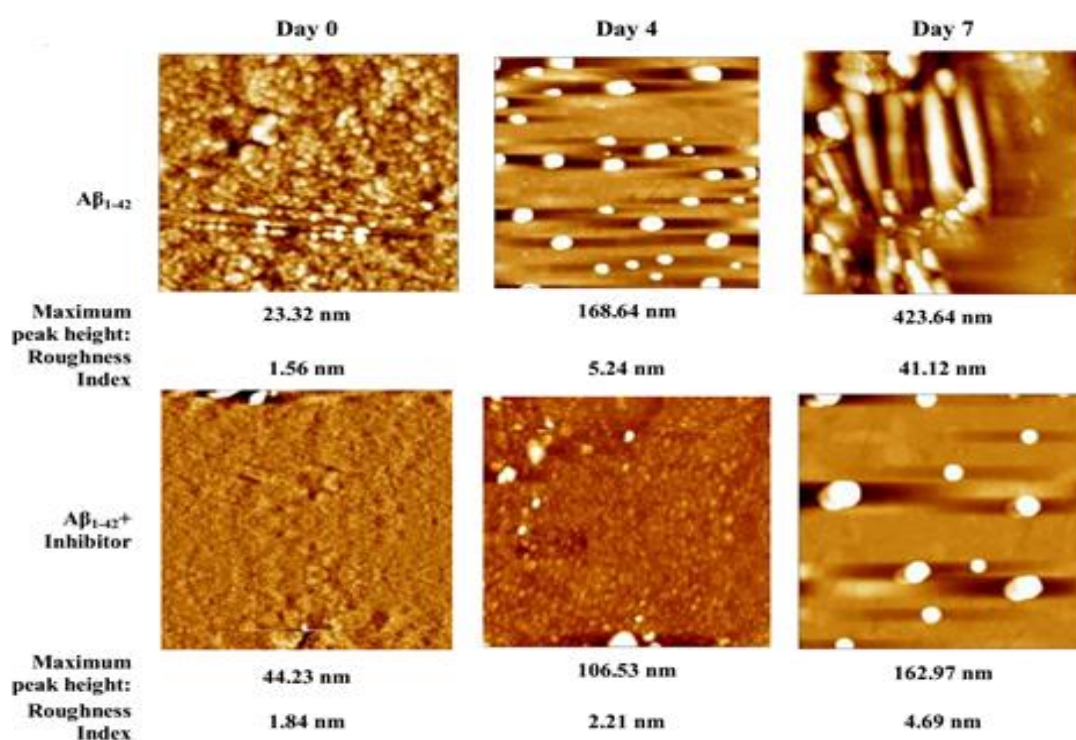


**Figure 5.17.** AFM visualized images at 5  $\mu$ m scale for the sample of A $\beta$  in the presence or absence of inhibitor **13o** over 7 days.

#### 5.2.2.1.7 Neuroprotection studies on SH-SY5Y cell line

The neuroprotective activity was determined against human neuroblastoma SH-SY5Y cell lines using 3-(4,5-dimethylthiazol-2-yl)-2,5-diphenyl tetrazolium bromide (MTT) assay [More and Vince 2012]. The activity was performed using four different concentrations of test compounds in the range of 10–80  $\mu$ M to determine their efficiency

in detecting cell death against A $\beta$ -induced oxidative stress. In this assay, 20  $\mu$ M of A $\beta$  was incubated with SH-SY5Y cells to attenuate the percentage cell viability to 61% compared to control. The results demonstrated augmented cell viability by test compounds (**13n**: 63–83%; **13o**: 69–89%) in a dose-dependent manner. Overall results suggested the neuroprotective activity of compounds **13n** and **13o** against A $\beta$ -induced oxidative stress in SH-SY5Y neuroblastoma cell lines (Figure 5.18).

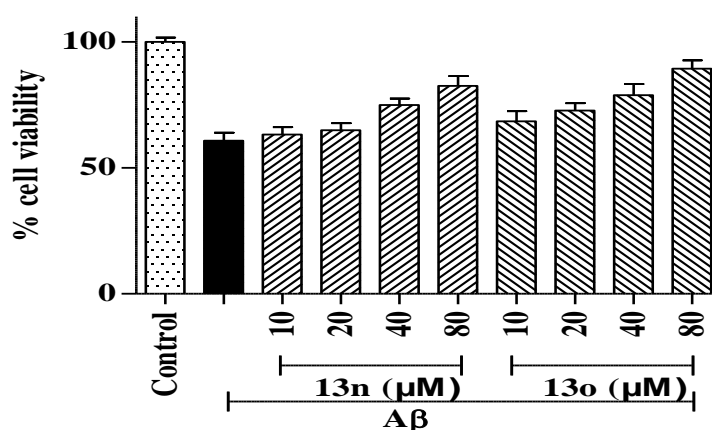


**Figure 5.18.** Neuroprotective activity of compounds **13n** and **13o** against A $\beta$ -induced oxidative stress in SH-SY5Y cell lines by MTT assay. Each bar displays the values of % cell viability as the mean  $\pm$  SEM of three separate experiments (n = 3).

### 5.2.2.2 *In-vivo* behavioral studies

#### 5.2.2.2.1 *Acute oral toxicity study*

The acute toxicity was evaluated as per OECD guidelines 425 on healthy female Wistar rats. Compounds **13n** and **13o** were well tolerated and showed no sign of abnormal reactions or toxicity at the graded doses of (677, 1333, 2000 mg/kg), p.o. up to 14 days of testing. The results suggested that tested compounds possessed a significant margin of safety and can be processed for *in-vivo* investigations in rats.

#### 5.2.2.2.2 *Scopolamine-induced amnesia model: Y-maze test*

The *in-vivo* efficacy of compounds **13n** and **13o** to ameliorate scopolamine-induced cognitive dysfunction was evaluated by Y-maze test in healthy male Wistar rats.

Scopolamine is a common drug used to induce cognitive dysfunction due to cholinergic deficit [Klinkenberg and Blokland 2010]. The donepezil was used as standard (5 mg/kg, p.o.) and the compounds (**13n** and **13o**) were evaluated at different dose levels (2.5, 5, and 10 mg/kg, p.o.). The results of sequential arm entries, i.e., spontaneous alternation score (% alteration) were calculated along with total arm entries of respective animals [Lalonde 2002]. The cognitive deficit was induced by the administration of scopolamine affirmed by a significant reduction in % spontaneous alternation (Figure 5.19A,  $###p < 0.001$ ) compared to control. The treatment with donepezil displayed significantly higher (Figure 5.19A,  $***p < 0.001$ ) % spontaneous alternations compared to scopolamine. Further, the treatment with test compounds **13n** and **13o** demonstrated improvement in scopolamine-induced cognitive deficit in a dose-dependent manner with maximum activity was observed at 10 mg/kg. The treatment of **13n** and **13o** showed significantly higher % spontaneous alternations (Figure 5.19A,  $***p < 0.001$ ) compared to scopolamine. Interestingly, compound **13n** (10 mg/kg) and **13o** (5 and 10 mg/kg) demonstrated statistically non-significant difference in % spontaneous alternation (Figure 5.19A, ns) than donepezil. Moreover, similar total arm entries of all the groups (Figure 5.19B, ns) ascertained that scopolamine didn't impede the locomotive behavior in animals during the experiment.

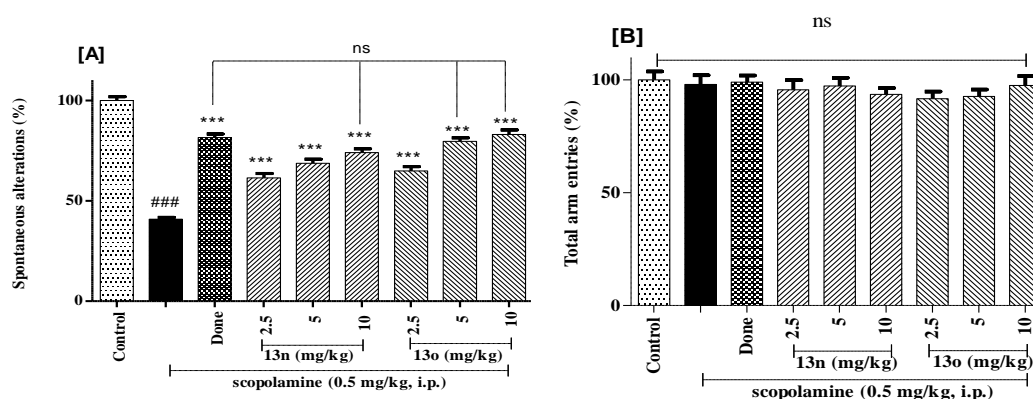


**Figure 5.19.** The effect of compounds **13n** and **13o** (2.5, 5, 10 mg/kg) in Y-maze test

[A] % spontaneous alternation; [B] total arm entries. Data are expressed as the mean  $\pm$  SEM (n = 6); ### p < 0.001 vs control; \*\*\* p < 0.001 vs scopolamine; ns = non-significant; DONE = donepezil.

#### 5.2.2.2.3 A $\beta$ -induced AD phenotypic model: Morris water maze test

Morris water maze test was performed to evaluate the improvement by A $\beta$ <sub>1-42</sub>-induced cognitive dysfunctions in the AD rat model [Zhou et al. 2012]. The intracerebroventricular (ICV) administration of A $\beta$  reported producing the most common phenotypic conditions of AD [Wang et al. 2015]. The results of Morris water maze experiment were reported as escape latency time (ELT), i.e., the time required reaching the hidden platform and numbers of platform crossovers during 90 seconds of trial. The decline in ELT and an increase in the numbers of platform crossovers were considered as a mark of improvement in learning and memory over five days. The ELT was increased significantly (Figure 5.20A), while the number of platform crossovers progressively declined (Figure 5.20B) in the model group of animals compared to the sham group, which confirmed the induction of cognitive impairment with ICV administration of A $\beta$ . The ELT was remarkably reduced (Figure 5.20A), while platform crossovers were observed to be significantly higher (Figure 5.20B) with the administration of donepezil and compound **13o** compared to the model group. Interestingly, compound **13o** exhibited slightly better efficacy in improving learning and memory impairment than donepezil. Overall results of behavioral investigation elicited significant potential of compound **13o** in improving cognitive dysfunctions. Moreover, results are observed in agreement with *in-vitro* assays.

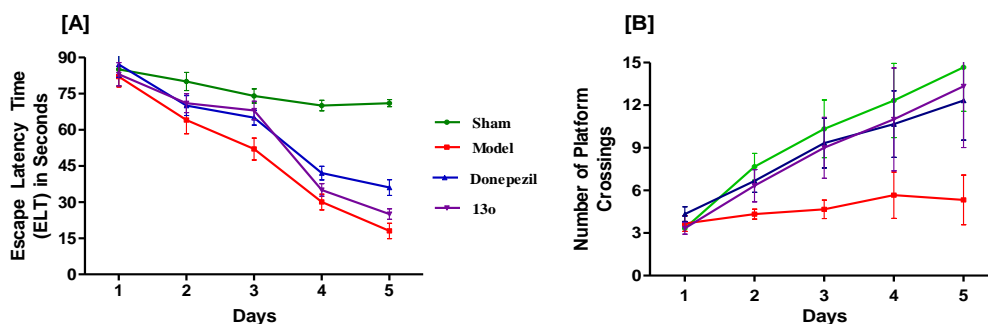


**Figure 5.20** Assessment of improvement in learning and memory impairment by compound **13o** in Morris water maze test; (A) escape latency time (ELT); (B) numbers of platform crossings. Data are expressed as the mean  $\pm$  SEM (n = 6).

### 5.2.2.3 *Ex-vivo* study

The effect of compounds **13n** and **13o** on AChE level in hippocampal brain homogenates was determined by Ellman's method [Ellman et al. 1961]. Scopolamine treated group (model) showed significantly higher levels of AChE as compared to the control group (sham). Compounds **13n**, **13o**, and donepezil significantly reduced (Figure 5.21A,  $###p < 0.001$ ) the rate of ACh hydrolysis via inhibition of brain AChE as compared to scopolamine group. The *ex-vivo* study revealed that compounds **13n** and **13o** (10 mg/kg) has remarkably increased AChE activity (Figure 5.21A,  $***p < 0.001$ ) by reducing the rate of substrate hydrolysis compared to the scopolamine group. The results also indicated the non-significant differences (Figure 5.21A, ns) in AChE activity of compound **13n** and **13o** (10 mg/kg) with donepezil.

The oxidative stress is a primary instigator of clinical and pathological AD [Bonda et al. 2010]. The malondialdehyde (MDA) and superoxide dismutase (SOD) are major biochemical markers of oxidative stress. Thiobarbituric acid-reactive substances (TBARS) assay was performed to estimate the level of MDA in the sample of hippocampal brain homogenates. The results indicated that MDA levels were significantly elevated (Figure 5.21B,  $###p < 0.001$ ), while SOD activity was substantially attenuated (Figure 5.21C,  $###p < 0.001$ ) in the scopolamine treated group compared to control group. The MDA level was remarkably declined (Figure 5.21B,  $***p < 0.001$ ),

while SOD activity was increased significantly (Figure 5.21C,  $*** p < 0.001$ ) by treatment with compounds **13n** and **13o** (10 mg/kg) than scopolamine group, which confirmed its antioxidant potential.

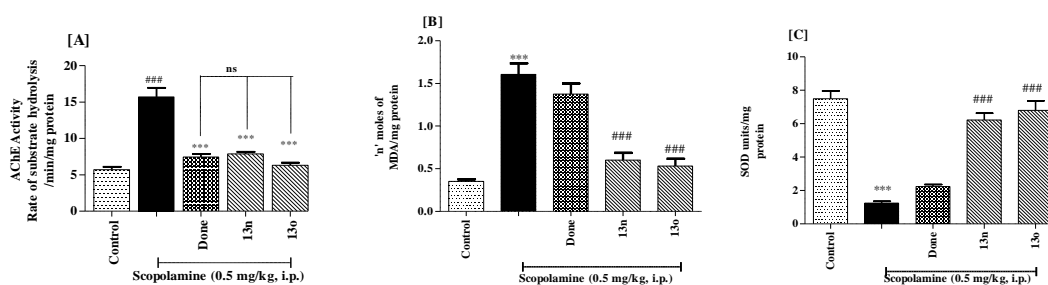


**Figure 5.21** The *ex-vivo* and biochemical analysis of compounds **13n** and **13o** in hippocampal brain homogenates; [A] AChE activity; [B] level of MDA in TBARS assay and; [C] SOD activity. All the values are represented as the mean  $\pm$  SEM ( $n = 6$ ); ###  $p < 0.001$  vs control; \*\*\*  $p < 0.001$  vs scopolamine; ns = non-significant; Done = donepezil.

#### 5.2.2.4 Pharmacokinetic study

Preliminary pharmacokinetic analysis was performed to establish a point to point the correlation between *in-vitro* and *in-vivo* results. The most potent compound **13o** was orally administered at a dose of 10 mg/kg in healthy male Wistar rats. Blood samples were collected from retro-orbital plexus at several time points (See Experimental Section). The results were analyzed by the extravascular non-compartment model using Kinetica software (Thermo Fisher Scientific, version 5.0.11). The results of the pharmacokinetic experiment suggested that maximum plasma concentration ( $C_{\max} = 49.78$  ng/ml) was achieved at 5.33 h ( $T_{\max}$ ). The half-life ( $t_{1/2}$ ) of compound **13o** was observed to be 12.31 h, while mean residence time was 18.35 h. Overall results demonstrated the excellent absorption and bioavailability of compound **13o** following an oral administration. The results are summarized in Table 5.6.

**Table 5.6.** Pharmacokinetic evaluation after an oral administration of **13o** (10 mg/kg, p.o.)

Parameters	Effect of <b>13o</b> *
$C_{\max}$ (ng/mL)	$49.78 \pm 2.39$

---

$T_{\max}$ (h)	$5.33 \pm 1.33$
$(AUC)_{0-24}$ (ng/mL <sup>*</sup> h)	$721.15 \pm 9.35$
$t_{1/2}$ (h)	$12.31 \pm 1.43$
MRT (h)	$18.35 \pm 2.08$

---

<sup>\*</sup>All values are expressed as mean  $\pm$  SEM (n = 3).

### 5.2.3 Computational studies

#### 5.2.3.1 *In-silico* molecular docking study

To gain insights into the interaction of compound **13o** with the active site residues of hAChE and hBACE-1, molecular docking studies were undertaken using Schrödinger Glide Program. The compound **13o** was docked using Glide XP module, and the results were visualized using XP visualizer tool. The results of docking studies on hAChE revealed that compound **13o** interacted effectively with PAS residues and extended into the deep gorge of CAS (Figure 5.22A). The oxadiazole nucleus formed electrostatic and face-to-face  $\pi$ - $\pi$  stacking interactions with Asp74 and Tyr341, respectively at PAS region, whereas Tyr124 and Trp286 residues of PAS were involved in hydrophobic interactions with the 2-pyridyl piperazine ring. The 2-pyridyl N-atom of compound **13o** form H-bonding with Phe295 at acyl binding pocket of hAChE. The molecule was extended deep into CAS via anionic subsite and oxyanion hole and interacted effectively with Trp86 (hydrophobic), Glu202 (electrostatic), and Phe338 (hydrophobic) residues at anionic subsite. While at oxyanion hole glycine interactions were observed with Gly120, Gly121, and Gly122 residues. Moreover, compound **13o** was observed to occupy the deep gorge of CAS, and terminal 2,4-difluorophenyl group interacted with Ser203 and His447 residues with polar and face-to-face  $\pi$ - $\pi$  stacking interactions, respectively (Figure 5.23A).

Additionally, the binding mode interaction of compound **13o** was observed on hBACE-1 (2ZJM) and presented in Figure 5.22B. The results of docking on hBACE-1 demonstrate that compound **13o** interacted effectively with catalytic dyad residues



(Asp32 and Asp228) (Figure 5.23B). The N-atom of 2-pyridylpiperazine nucleus contacted with Asp32 through H-bonding and salt bridge formation, while oxadiazole and terminal phenyl group interacted electrostatically with Asp228 (Figure 5.22B).

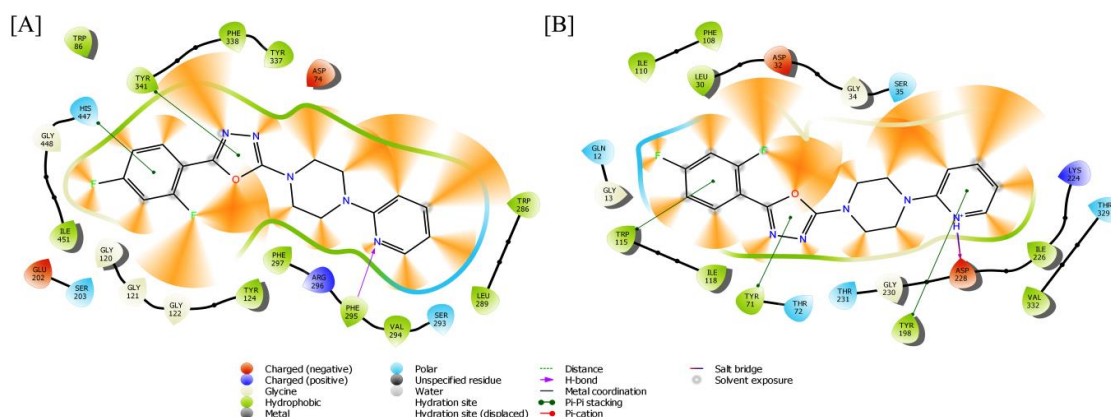


**Figure 5.22.** 2D docked pose of compound **130** on; [A] hAChE (4EY7) and; [B] hBACE-1 (2ZJM).

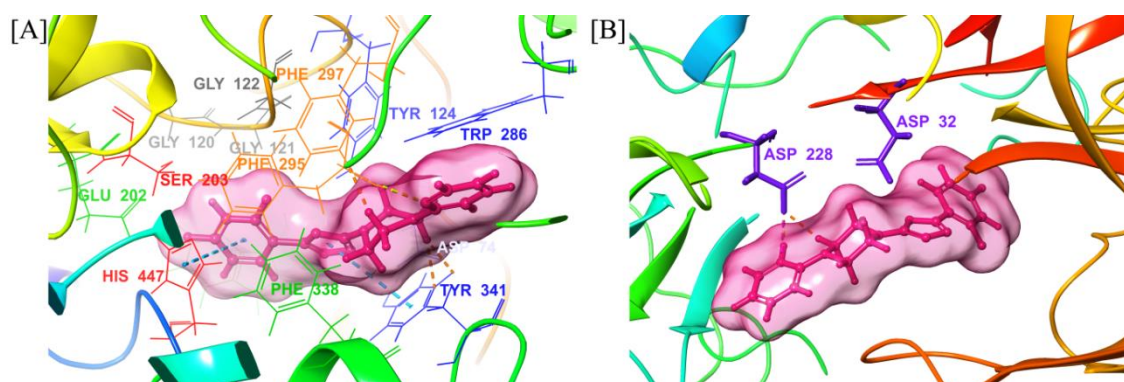


**Figure 5.23** Docking poses of compound **130** in active sites of; [A] hAChE (4EY7); The peripheral anionic site (PAS) residues are indicated as blue (Tyr72, Tyr124, Trp286, and Tyr341), catalytic active site (CAS) as red (Ser203, His447, and Glu334), anionic subsite as green (Trp86, Glu202, and Phe338), acyl binding pocket (ABP) as orange (Phe295 and Phe297), and oxyanion hole as grey (Gly120 and Gly121). [B] hBACE-1 (2ZJM); Aspartate dyad (Asp32 and Asp228) residues are showing as purple. Compound **130** is showing as pink with surrounding active bound surface.

### 5.2.3.2 Molecular dynamics simulations study

The molecular dynamics simulation study of 40 ns run was performed to affirm the stability of docked complexes of **130** against both the targets, i.e., hAChE and hBACE-1. The RMSD values for each simulation run were calculated to measure the stability of protein-ligand poses relative to protein backbone structure, and the results suggested that conformational changes in all the docked complexes were well within the

acceptable limit of 1–3 Å (Figures 5.24A and 5.24B) during the simulation run of 40 ns. The ligand-protein interactions were visualized by 2D-graphics, histograms, and time-line representations.

The simulation analysis of **13o**-hAChE docked complex suggested that binding of the molecule at PAS region was stable, while interactions at CAS residues were not observed. The terminal 2,4-difluorophenyl group interacted at PAS, via face-to-face  $\pi$ - $\pi$  stacking interaction with Trp286 (56%), while Tyr341 interacted hydrophobically. At anionic subsite, 2-pyridyl nucleus formed  $\pi$ - $\pi$  stacking interaction with Trp86 (35%), and hydrophobic interaction of Phe338 also remained stable (Figures 5.25A–C). The docked pose analysis of compound **13o** on hBACE-1 displayed stable and significant interactions with catalytic dyads (Asp32 and Asp228). The N-atom of 2-pyridylpiperazine nucleus contacted through H-bonding with Asp32 (21%) and Asp228 (96%) (Figures 5.26A–C). Overall results of molecular dynamics simulations showed consensual binding interactions of compound **13o** with PAS-AChE and aspartate dyad of BACE-1.

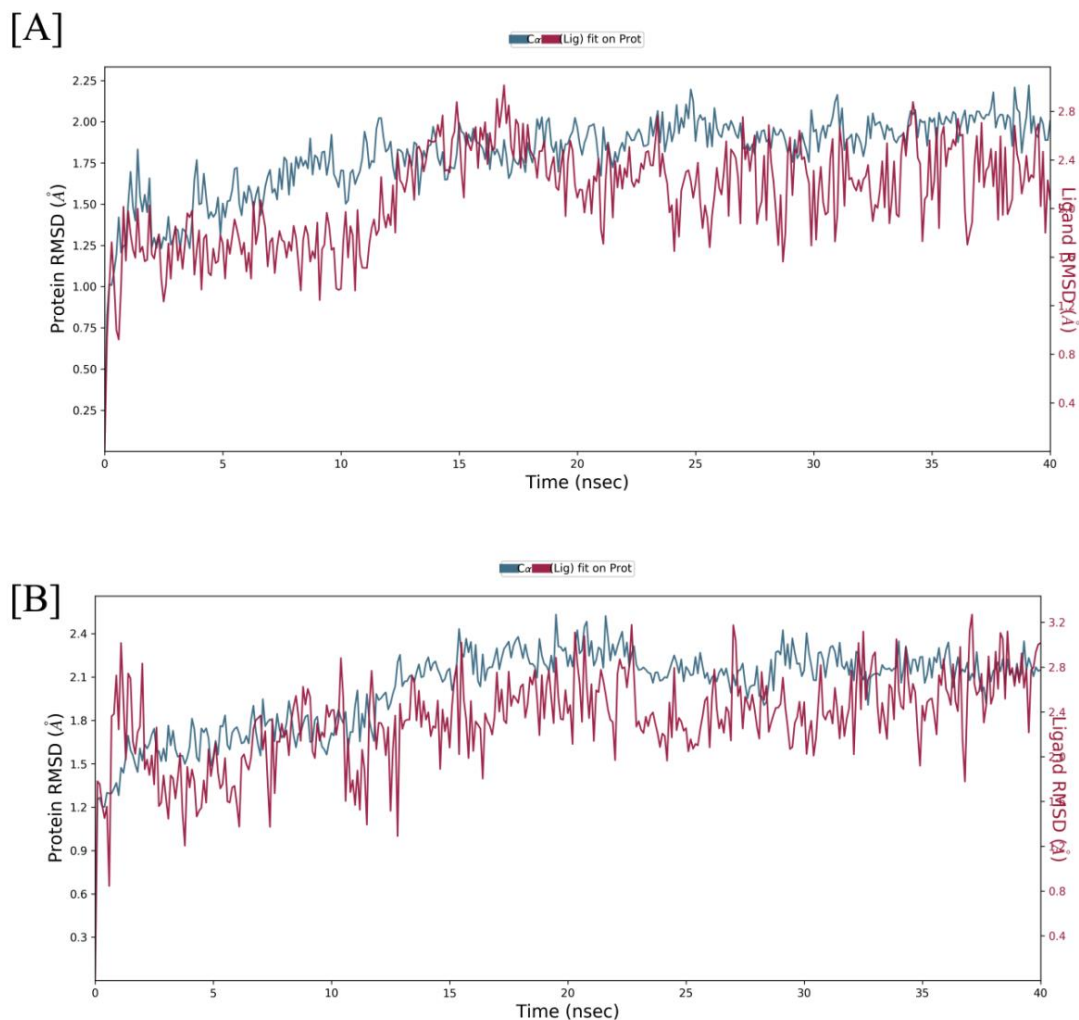


**Figure 5.24.** The ligand-protein RMSD relative to protein backbone structure for compound **13o** against; [A] hAChE (4EY7) and; [B] hBACE-1 (2ZJM).

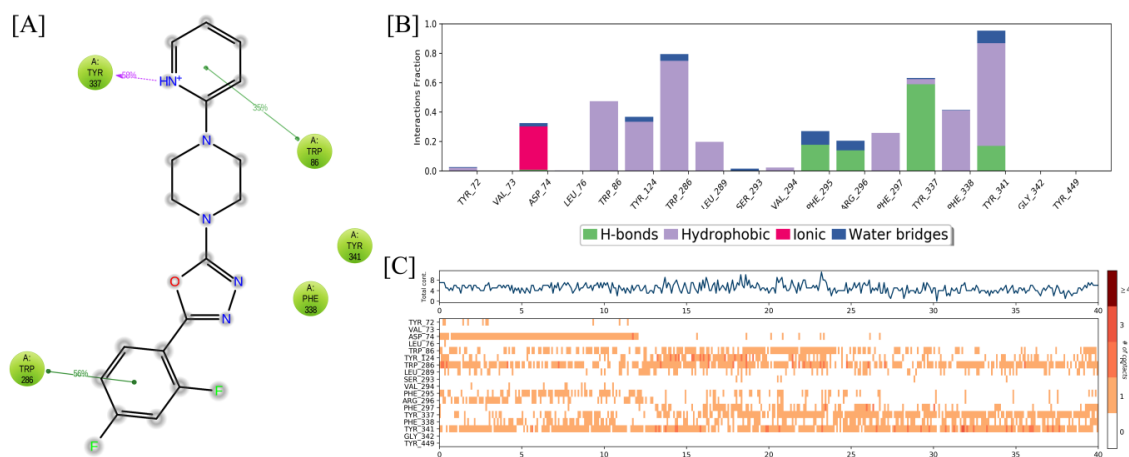


**Figure 5.25** Molecular dynamics simulation study of the docked complex of **13o**-hAChE; [A] graphical representation showing percentage interaction; [B] histogram showing interaction fractions; [C] time-line representation showing active site binding interaction with each amino acid residues for a total simulation run time of 40 ns.

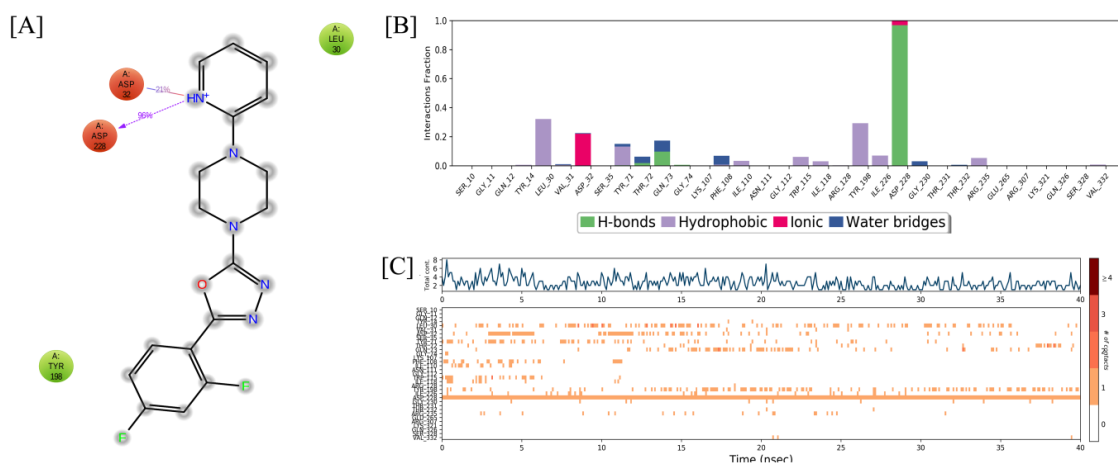


**Figure 5.26** Molecular dynamics simulation study of the docked complex of **130-hBACE-1**; [A] graphical representation showing percentage interaction; [B] histogram showing interaction fractions; [C] time-line representation showing active site binding interaction with each amino acid residues for a total simulation run time of 40 ns.